Chemistry Europe
European Chemical Societies Publishing

Special Collection

Photocatalytic Nitrogen Reduction: Challenging Materials with Reaction Engineering

Dirk Ziegenbalg,*[a] Judith Zander,[b] and Roland Marschall*[b]

Ammonia is not only the most important chemical for fertilizer production, it has also gained much interest as a future hydrogen storage material. Besides the well-known Haber–Bosch process to generate ammonia from elemental sources, new ways to convert nitrogen into ammonia have been investigated in the last decade for a decentralized production, including electrocatalytic and photocatalytic approaches. However, photocatalysis in particular suffers from stagnating materials development and unstandardized reaction conditions. In this Review, we shine light on recent materials and reaction engineering results for photocatalytic nitrogen reduction, putting an emphasis on the need to connect the activity of reported materials together with detailed reaction conditions and efficiencies. Photocatalytic nitrogen reduction is an emerging field that will certainly gain significant interest in the future as a sustainable pathway to generate green hydrogen and ammonia. The field will certainly strongly benefit from joint efforts with strong interactions between chemists, physicists and chemical engineers at a fundamental level.

1. Introduction

Industrial ammonia production as first step of fertilizer production is the foundation to feed almost half of the global population (Figure 1).[1] The production of ammonia is associated with a significant energy use of more than 1% of the global consumption of fossil energy and consequently contributes to more than 1% of the global greenhouse gas emissions.[2,3] It is foreseeable that the ever growing world population will cause a further increase of the demand for ammonia. In the context of energy transition, chemical energy carriers are required to replace common fossil fuels. Ammonia is highly attractive as sustainable energy carrier that can be used in combustion engines as well as fuel cells.

The tremendous impact of ammonia production on society and climate calls for the development of alternative manufacturing technologies with a smaller or zero CO_2 footprint. Consequently, various concepts are currently under investigation to reduce the CO_2 footprint, focusing on different steps of the conventional ammonia synthesis. The main research interest is on hydrogen production, replacing conventional steam methane reforming.[2] Beside conventional hydrogen production with reduced CO_2 emissions through coupling to e.g. carbon capture and storage concepts (blue ammonia), green ammonia production focusses on the production of hydrogen through electrolysis of water with renewable electrical energy or from biomass coupled to carbon capture and storage.

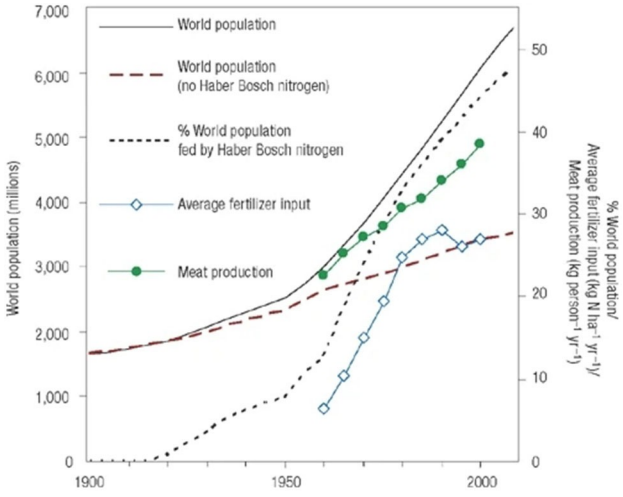

Figure 1. Development of ammonia production and world population. Reproduced with permission from Ref. [1]. Copyright (2008) Springer Nature.

The direct use of solar irradiation for N_2 conversion is a highly desirable but challenging approach.[4] Decentralized on-site production of ammonia for further conversion to fertilizers was identified as attractive concept that was economically feasible for photovoltaic powered production plants already in 2015.[5] Even more recent, the photocatalytic pathway has gained increasing attention, a research field that is in its infancies. A variety of photocatalytic materials is currently under research, raising issues to comparability and derivation of overarching insights. To fill this gap, this review analyses the

[a] Prof. Dr. D. Ziegenbalg
Institute of Chemical Engineering
Ulm University
Albert-Einstein-Allee 11, 89081 Ulm (Germany)
E-mail: dirk.ziegenbalg@uni-ulm.de
[b] J. Zander, Prof. Dr. R. Marschall
Department of Chemistry
University of Bayreuth
Universitätsstrasse 30, 95447 Bayreuth (Germany)
E-mail: roland.marschall@uni-bayreuth.de

Special Collection An invited contribution to the "GDCh and ChemPhotoChem: 5-Year Anniversary" Special Collection.

current progress with respect to concepts of material development and reaction engineering.

2. Challenges of N_2 Activation

2.1. General Aspects

Nature enables the conversion of N_2 in a similar scale as artificial N_2 conversion is conducted. Herein, especially nodular bacteria allow to convert 50–150 kg air per hectare and present a unique decentralised but yet industrially hardly usable source for N_2 conversion. N_2 conversion in biological systems is performed under much milder conditions as in the industrial Haber-Bosch process, using the metalloenzyme nitrogenase, which allows for the reduction of N_2 to ammonia. Several bacteria depend on nitrogenase enzymes for their nitrogen supply.[6] Examination of the active site of nitrogenase revealed a co-factor constructed of mainly sulphur, iron and molybdenum atoms with an interstitial carbon atom (Figure 2).[7] The chemical energy required for this reaction is delivered by the hydrolysis of ATP (adenosine 5′ triphosphate).[8] A second, Fe-based component of the enzyme, in which ATP hydrolysis takes place, delivers the electrons required. The total reaction involves the transfer of eight electrons, according to Equation (1):[6]

$$N_2 + 8\ e^- + 16\ ATP + 8\ H^+ \rightarrow 2\ NH_3 + H_2 + 16\ ADP + 16\ P_i \quad (1)$$

Herein, the difficulty of cleaving the N_2 triple bond, possessing an extremely high dissociation enthalpy of ~945 kJ mol^{-1} or ~10.0 eV, is circumvented by its activation at the co-factor and thus increasing the Lewis acid/base activity of

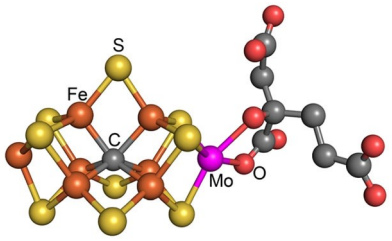

Figure 2. Depiction of the Mo- and Fe-containing cofactor at the active site in nitrogenase. Reproduced with permission from Ref. [7]. Copyright (2018) The American Association for the Advancement of Science.

N_2.[9] This in turn also facilitates its reduction and protonation. The activation is consequently a result of electron back donation from metal centres to the antibonding π^* orbitals of N_2.[10]

Noteworthy, "artificial photosynthesis", which takes the natural photosynthesis and the involved catalyst structures as an example and either directly or indirectly substituting biological steps by chemical routes, has become a widely researched topic and is generally accepted as a valuable idea (although the overall energy efficiency is still far behind natural photosynthesis). The same is possible for "artificial N_2 conversion" with photocatalytic methods.

While being thermodynamically challenging, light-driven nitrogen reduction is thermodynamically more favorable than water splitting.[11] Already in the 1940s TiO_2, Fe_2O_3 or ZnO_2 were identified as active photocatalysts for N_2 photoreduction.[12] These materials are very common in desert soils and it is estimated, that up to 10^7 tons of N_2 are photoreduced in this manner every year. These catalysts can in theory produce ammonia based on air and water [Equation (2)]:[11]

Dirk Ziegenbalg studied chemistry at Friedrich-Schiller-University Jena from where he graduated with a PhD in Industrial Chemistry in 2013. In 2012 he moved to University Stuttgart to start a research group at the Institute of Chemical Technology. He holds a M.Sc. degree in Economics from the Friedrich-Schiller-University Jena. In 2018 he was appointed professor at the Institute of Chemical Engineering of Ulm University. His research interests focus on photochemical reaction engineering at the interface between chemical engineering, microreaction technology and photochemistry.

Judith Zander received her B.Sc. (2017) and M.Sc. (2020) from the University of Bayreuth. She is currently a PhD student in the research group of Prof. Dr. Roland Marschall, where she is working on semiconductor materials and composites for photocatalytic and electrochemical applications, with a focus on the nitrogen reduction reaction.

Roland Marschall studied chemistry at the University of Hannover from where he obtained his PhD in Physical Chemistry in 2008. After postdoctoral research stays at The University of Queensland, Fraunhofer ISC and Ruhr-University Bochum, he became Emmy-Noether Young Investigator at Justus-Liebig-University Giessen in 2013. Since 08/2018, he is full professor at the University of Bayreuth. His research interests include heterogeneous photocatalysis using mesostructured semiconductor mixed oxides for water splitting, CO_2 reduction and N_2 reduction. He coordinates the upcoming DFG Priority Programme SPP 2370 "Nitroconversion".

$$N_{2\,(g)} + 3\,H_2O_{\,(g)} \rightarrow 2\,NH_{3\,(g)} + 1.5\,O_{2\,(g)}\ \Delta_r H = 633.2\,kJ\,mol^{-1} \quad (2)$$

This reaction can be divided into two half-reactions. At pH = 0, ammonia in aqueous solution is present as ammonium [Equations (3), (4)]:[13]

$$3\,H_2O_{(l)} \rightarrow 1.5\,O_{2(g)} + 6\,H^+{}_{(aq)} + 6\,e^-\ E^0_{SHE} = 1.23\,V \quad (3)$$

$$N_{2(g)} + 8\,H^+{}_{(aq)} + 6\,e^- \rightarrow 2\,NH_4{}^+{}_{(aq)}\ E^0_{SHE} = 0.274\,V \quad (4)$$

Thus, theoretically the reaction should be possible on semiconductor photocatalysts with a band gap larger than ~1 eV and appropriate band locations. It is also noticeable that the potential for hydrogen evolution (0 V at pH = 0) is not much higher than that of nitrogen reduction. Furthermore, the reduction of one molecule of N_2 necessitates the transfer of 6 electrons, something that can end up in rate determining steps, favouring *e.g.* the formation of H_2, especially in photocatalysis and photoelectrochemistry. Therefore, catalysts are needed to overcome this activation barrier due to charge accumulation. The O_2 evolution reaction (OER) moreover usually requires rather high overpotentials. Overall, the situation is similar to CO_2 reduction reactions via multi-electron transfer. This leads to the problem that nitrogen reduction, as does CO_2 reduction, competes with hydrogen evolution reaction, and the selectivity towards ammonia is a major challenge.[11] The low solubility of N_2 in water, the most often used reaction medium, is also a limiting factor as the surface coverage of a given catalyst with water, protons and N_2 as such will already be an intrinsic hindrance to achieve high ammonia selectivity.

The reaction is very endothermic.[11] Schrauzer observed the occurrence of hydrazine, leading to the suggestion of a sequential reduction via N_2H_2 and N_2H_4.[14] Even though the first reaction step is also highly endothermic, the free energy per electron is with 2.5 eV significantly smaller than the band gap of TiO_2. It was found that water vapor enhances the activity, as do sacrificial agents under certain conditions. Ideal reaction temperatures are between 80 and 120 °C.[11] The first step in the reduction of adsorbed nitrogen is the transfer of an electron and a proton to N_2 to create a HN=N• species. It is not yet fully clear what steps proceed afterwards, but it is believed that either proton or electron transfer occur consecutively at one nitrogen, liberating ammonia and leaving one N behind, or that the transfer proceeds alternatingly at both N (Figure 3).[15] The two proposed reaction pathways for N_2 hydrogenation are the associative and dissociative pathway, which can be distinguished by the sequence of breaking the N≡N bond.[16]

For more details on specific aspects of NRR, we suggest the readers some of the excellent specific reviews and articles out there covering multiple aspects of general N_2 activation.[17–22]

2.2. Present Materials and Common Strategies to Improve Performance

Different strategies have been explored to boost the photocatalytic activity for the photocatalytic nitrogen reduction reaction (NRR). In general, either the photophysical, surface properties or a combination of both are modified to achieve high performance by e.g. introduction of surface defects,[23,24] plasmonic sensitization,[25] doping,[26,27] addition of cocatalysts,[28,29] or the development of heterojunctions.[30,31] The following sections elaborate on some photocatalytic materials for N_2 conversion and design strategies. Quantitative performance data will not be reported in this section. Instead, a comprehensive quantitative overview of the reviewed literature will be given afterwards in a separate section.

Photocatalytic N_2 reduction has been demonstrated for a variety of material classes such as metal oxides, nitrides, sulfides, carbon nitrides or layered double hydroxides.

2.2.1. Metal Oxides

As mentioned above, already in the 1940s TiO_2, Fe_2O_3 or ZnO were identified as potential photocatalysts for N_2 photoreduction.[12,14]

A lot of research focused on the use of TiO_2.[14,32–34] However, pure TiO_2 does not show any activity, although annealing at high temperatures and thereby introduction of defects induces activity. Contrary to water splitting, rutile shows high activity compared to anatase (Figure 4). Moreover, TiO_2(B) has been shown to exhibit activity for dinitrogen conversion to ammonia.[35] Rutile possesses a high overpotential for hydrogen evolution and a low overpotential for nitrogen reduction.

Detailed mechanistical studies were conducted by Thiel and co-workers with density functional calculations for N_2 reduction to NH_3 on the rutile TiO_2 (110) surface containing oxygen

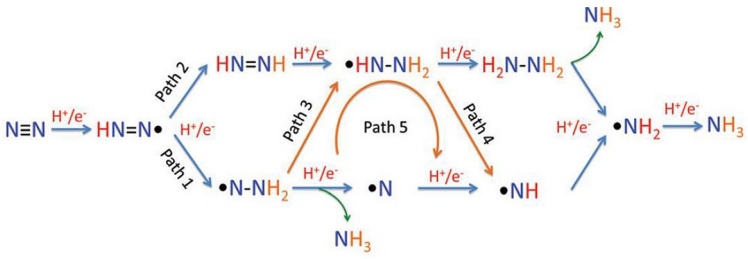

Figure 3. Proposed pathways of nitrogen reduction. Reproduced with permission from Ref. [15]. Copyright (2018) Royal Society of Chemistry.

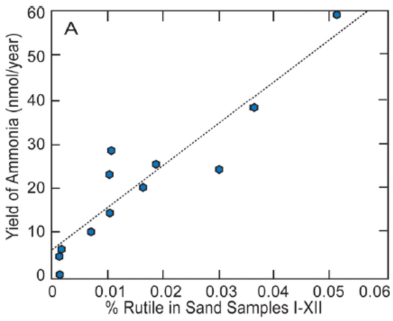

Figure 4. Dependence of ammonia production on rutile content. Reproduced with permission from Ref. [11]. Copyright (2017) The American Chemical Society.

vacancies driven by the photolysis of adsorbed water. The overall reaction from N_2 adsorption to NH_3 was found to be exothermic by ~2.0 eV. Three H_2O photolysis events provide the energy to pass the barriers (0.4–1.3 eV) of the each single step. In spite of the high bond strength of the N–N triple bond, N_2 conversion on TiO_2 is a downhill process.

Generally, much research has been focused on the introduction of surface defects to improve nitrogen adsorption. Oxygen vacancies have been induced in TiO_2, which improve the activity without the need for noble metals.[36] Hirakawa et al. used commercial TiO_2 in phosphate or water/alcohol mixtures to reduce N_2 gas photocatalytically. Natural Ti^{3+}-defects on a crystalline TiO_2 surface cleaved the N–N triple bond, reduced TiO_2 showed no activity. Only NH_3 was detected.[33] Wang et al. prepared defect-controllable TiO_2 nanotubes through annealing under a hydrogen atmosphere and a subsequent amine-assisted remedying strategy to generate oxygen vacancies. An optimal density of defects extends the visible light absorption and inhibits recombination.[37] Gong et al. grew TiO_2 nanorods on fluorine-doped tin oxide (FTO) by hydrothermal synthesis, then covering them with plasmonic gold nanoparticles and a thin TiO_2 layer *via* atomic layer deposition (ALD). The amorphous ALD-derived layer could promote N_2 adsorption and activation, greatly enhancing the N_2 photofixation rate. Because of the surface growth mechanism of ALD, oxygen vacancies could be confined at the very surface region of TiO_2 without affecting the bulk properties.[38]

Medford and Comer elaborated whether oxygen vacancies or Fe substitutions act as active sites for N_2 reduction on rutile TiO_2(110). It was found that bridging oxygen vacancies significantly stabilize NH_x, indicating that breaking the N–N is thermodynamically possible on rutile (110). The reaction follows an oxidative pathway, benefiting from the strong oxidative driving force of the photogenerated holes. The authors hypothesize that an oxidized NO* intermediate is involved in the photocatalytic nitrogen reduction on rutile (110).[39]

Other dopants can force the formation of oxygen defects. Zhang et al. doped Cu into TiO_2 nanosheets to generate stress in the lattice for defect generation for strong chemisorption and activation of molecular N_2 and water.[40]

Oxygen vacancy and F were introduced on the TiO_2 nanoparticle surface by Guan et al.,[41] both facilitating chemisorption of nitrogen on the TiO_2 surface.

Cocatalysts like Au, Ru, Rh, Pd and Pt were also added to TiO_2 photocatalysts for nitrogen conversion. Loading with ruthenium proved to deliver the best results.[42] The optimal loading depended on the respective metal. Ammonia production was especially high if cocatalysts showed high M–H bond strength, and thus a high overpotential for hydrogen evolution.[42] This in turn signifies that they act more as suppressors of hydrogen evolution than promoters of ammonia production. Using photodeposited Au nanocrystals as cocatalyst, Chang and Xu used electrospun TiO_2 nanotubes for nitrogen conversion, indicating that the photodeposition also helps generating oxygen vacancies for chemisorption of dinitrogen.[43] Liu et al. used the oxygen vacancies in TiO_2 nanosheets for single Ru atom decoration for photoreduction of aqueous N_2 to NH_3.[44] They concluded that such single atom catalyst might hinder the hydrogen evolution reaction, thus enhancing the selectivity of the photocatalytic N_2 reduction.

In a combined experimental and theoretical approach, Comer et al. investigated the role of adventitious carbon in photocatalytic N_2-conversion over TiO_2 by a combination of ambient-pressure X-ray photoelectron spectroscopy (AP-XPS) experiments and density functional theory (DFT) studies. According to them, adventitious surface carbon promotes photoinduced adsorption of N_2 at TiO_2 through the formation of metastable active sites by photooxidation of hydrocarbon species. Therefore, careful characterization and control of surface carbon is critical to ensure reproducibility in photocatalytic nitrogen fixation on TiO_2 and other semiconductors.[45] The results were later confirmed in aqueous photocatalytic nitrogen conversion.[46]

Yin et al. used alkali metal cations (Li^+, Na^+, and K^+) on Au/P25 to enhance N_2 photoconversion. Apparently, alkali metal cations can chemically promote nitrogen activation and promote ammonia evolution.[47]

Yu et al. decorated Au nanoparticles onto TiO_2 nanosheets. Oxygen vacancies on the TiO_2 nanosheets chemisorbed and activated N_2 molecules, which were subsequently reduced to NH_3 by hot electrons generated from plasmon excitation of the Au nanocrystals. Comparably, Jia et al. decorated Au nanorods with ceria (CeO_2) and Pt, and upon excitation of the localized surface plasmon resonance achieved nitrogen reduction with near-infrared light (upon methanol oxidation).[48]

Oshikiri et al. used tri-layer photoanodes of Au film on TiO_2 and Au nanoparticles in combination with a Zr cathode for aqueous photoelectrochemical nitrogen fixation.[49]

The success of utilizing oxygen vacancies to activate dinitrogen has been adapted to other metal oxides as well and transferred to nitrogen or sulphur vacancies in nitrides or sulphides, respectively.

Xiong et al. doped Mo into well-defined $W_{18}O_{39}$ nanowires to control the defect adsorption sites for N_2 bond dissociation.[26] Vu et al. doped Fe into $W_{18}O_{39}$ nanorods and

additionally decorated them with Au nanoparticles for photoelectrochemical nitrogen reduction.[50]

Hou et al. generated large amounts of grain boundaries in nanoporous WO_3, observing the formation of oxygen vacancies in the catalytic process. Ammonia production under light irradiation in water without any sacrificial agents was achieved.[51]

Oxygen vacancy-rich MoO_{3-x} nanobelts were used by Pan et al. for the formation of NH_4^+ from N_2. DFT calculations indicated that N_2 chemisorbs side-on on (001), while an end-on chemisorption occurs on the (100) plane. End-on chemisorption leads to an elongation of the bond length, which is critical for the activity.[52]

Wu et al. prepared defect-rich MoO_{3-x} nanosheets for plasmon-driven photochemical N_2 fixation, utilizing the co-existence of low-valent Mo^{5+} and oxygen vacancies for the activation of N_2 and the plasmon-induced generation of hot electrons, even in NIR (s. Figure 5).[53]

Chen et al. showed that amorphization-engineered cerium oxides (A-CeO_x) can be made with proper amount of oxygen vacancies with local electrons to function as active sites and carriers trap centers to endow excellent photocatalytic NH_3 synthesis performance.[54]

Regarding more complex oxides, $SrTiO_3$ and $BaTiO_3$ have been tested and it was found that addition of NiO increased their nitrogen activation,[55] and Fe-doped $SrTiO_3$ was shown to chemisorb and activate N_2 molecules effectively, and also promote the interfacial electron transfer from Fe-doped $SrTiO_3$ to N_2 molecules.[56] Bi_2MoO_6 also showed high activity in photocatalytic nitrogen fixation directly converting nitrogen from air.[57] Wang et al. used Bi-decorated $InVO_4$ for this reaction,[58] and Luo et al. used Fe-doped $SrMoO_4$.[59] Wu et al. used $Bi_3FeMo_2O_{12}$ nanoparticles for nitrogen fixation. The oxygen vacancies induced by hydrogen-treatments resulted in Mo^{5+} species, which can act as the active sites for nitrogen reduction.[60] CuCr-layered double hydroxides (LDH) nanosheets were used by Zhang et al. to reduce N_2 to ammonia in visible light. Here, the introduction of Cu(II) ions in the LDH nanosheets resulted in additional structural distortion and strain, leading to increased interaction between the LDH and N_2 promoting NH_3 evolution.[61]

Oxyhalides are another popular material class. N_2 absorption can occur efficiently on oxygen vacancies in bismuth oxybromide, activates the molecule and traps the electron. This leads to a high activity while noble metals or scavengers can be relinquished.[62] Hydrogenated BiOBr with strong surface disorder were synthesized by Zhang et al., showing a good nitrogen chemisorption.[63] Fe-doped BiOBr nanosheets were investigated by Liu et al. Oxygen vacancies are formed in the vicinity of Fe, leading to regions rich in photoexcited electrons. The π N–N antibonding orbital is populated by the 3d orbital electrons of Fe, finally activating the adsorbed N_2, leading to an increase of the N_2 fixation rate by eight times.[64] BiOBr (001) facets with different atomic terminations were studied by Ding et al. for their electronic structures and activation capacities, and checked their effect on the photocatalytic nitrogen fixation with DFT methods. It was found that Bi–Br facets can activate N_2 molecules effectively.[65] Br-doped BiOCl with large numbers of oxygen vacancies were synthesized by Wu et al.[66] Hou et al. investigated amorphous SmOCl nanosheets. Oxygen vacancies were identified to easily drive the dinitrogen reduction.[67] Furthermore, heterojunctions were studied for the nitrogen reduction reaction as well. Compared to single phase compounds, the activity generally increased. Typically, the light-absorber properties of TiO_2 are increased by composites like TiO_2/Fe_2O_3,[68] or TiO_2@C.[69] Heterojunctions of TiO_2 with C_3N_4 as the two of the most promising photocatalysts were studied for N_2 reduction as well.[69]

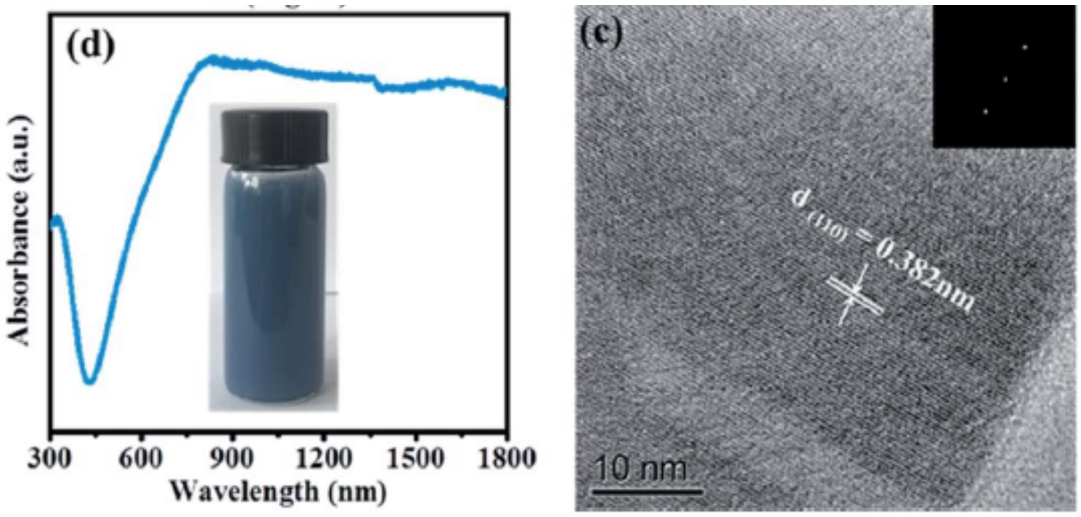

Figure 5. Blue MoO_{3-x} nanosheets for plasmon-driven photochemical N_2 fixation. Reproduced with permission from Ref. [53]. Copyright (2020) The Royal Society of Chemistry.

2.2.2. Metal Sulfides

Several sulfides have been applied in photocatalytic nitrogen conversion to ammonia. Sun reported on ultrathin electron-rich MoS_2 supporting sulphur vacancies, showing very high photocatalytic activity. The authors explained the efficiency with the existence of trions (one hole, two electrons), which enable simultaneous six electron transfer.[70] Sun et al. prepared a sulfur vacancy-rich O-doped 1T-MoS_2 nanosheets (SV-1T-MoS_2) and combined it with CdS nanorods to form a hybrid material (SV-1T-MoS_2/CdS). Compared with pure CdS nanorods and 1T-MoS_2/CdS composites without sulfur vacancies, the 30 wt.-% SV-1T-MoS_2/CdS photocatalyst exhibits excellent photocatalytic performance.[63,71] Light absorption by CdS nanorods was also used to promote an electron that is used by nitrogenase to reduce N_2.[8] Gao et al. decorated NiS onto CdS as a co-catalyst. Temperature-programmed desorption studies confirmed that the N_2 molecules preferred to adsorb onto the NiS/CdS surface, and the overpotential of the N_2 reduction reaction was also reduced by loading NiS.[72] Wang et al. prepared ZnS on graphene oxide for nitrogen conversion, which was much more active compared to ZnS alone.[73]

A MoS_2/C-ZnO composite was investigated by Xing et al. A high performance in photocatalytic N_2 reduction to NH_3 was recorded for irradiations with simulated sunlight. This result was reasoned by an efficient separation of charge carriers in addition to a large surface area.[74]

2.2.3. Carbon Nitrides

Recently, carbon nitrides have gained a lot of attention for photocatalytic nitrogen conversion. The best performance was achieved when N-vacancies were introduced into graphitic C_3N_4 (g-C_3N_4).[75] Those vacancies have received special attention in recent years, since the vacancies are of similar size like the N-atoms in dinitrogen. Hence, selective chemisorption should be feasible.[23] Defects can additionally influence the structure, as they can decrease the interlayer stacking distance due to a reduction of layer repulsion.[76]

Nitrogen vacancies could be introduced by calcining pre-synthesized g-C_3N_4 under nitrogen flow at 530 °C,[76] or by HCl treatment.[77] Jin et al. used dielectric barrier discharge plasma treatment to prepare N-deficient C_3N_4 for photocatalytic N_2 conversion. N vacancies act as chemical adsorption sites to activate nitrogen. A "two-path" ammonia production mechanism is proposed, in which H_2O_2 is included when air was used as reaction gas.[78] Due to the selective chemisorption of N_2, air can be used instead of pure N_2 without loss of activity.[76]

Comparably, Huang et al. prepared hollow and porous carbon nitride with nitrogen vacancies and oxygen doping for nitrogen conversion.[79]

KOH etching was reported to enhance the activity of bulk g-C_3N_4.[80] The reduction of N_2 was observed to proceed *via* a Mars-van-Krevelen mechanism. This means, that nitrogen in g-C_3N_4 is reacted to ammonia and resulting vacancies are replenished through nitrogen adsorption. K^+-modification can also contribute to an extended absorption capability of carbon nitride for photocatalytic nitrogen conversion and its cyano group regeneration at the surface.[81]

Zhang et al. generated carbon vacancies in carbon nitride sheets for nitrogen conversion to ammonia, and an effective charge separation from both bulk and surface was achieved.[82] Such carbon vacancies had the same effect as oxide vacancies in oxides, facilitating the chemisorption of N_2.

Wu et al. combined activation by nitrogen vacancies and plasmonic resonance absorption of Au nanoparticles on carbon nitride nanosheets for nitrogen conversion in pure water.[83]

As described earlier for TiO_2 oxygen vacancies, the nitrogen vacancies of carbon nitrides can also be used to deposit single atom catalysts for nitrogen reduction.[84] Especially iridium single metal atom catalysts showed a low activation barrier for nitrogen reduction.

Yuan et al. decorated graphitic carbon nitride with Ru/CoS_x with S-vacancies, resulting in asymmetric polarization of dinitrogen for its activation.[85]

Kong et al. modified graphitic carbon nitride with cyano-groups for better nitrogen chemisorption,[86] while Qiu et al. used salicylic acid modified graphitic carbon nitride for that.[87]

Nickel phosphide particles (Ni_2P) as cocatalyst were loaded on a boron-doped carbon nitride (BCN) by Shiraishi and co-worker. The valence band level was positively shifted by the doped B atoms, causing an enhanced water oxidation by the valence band holes. The excited electrons generated on BCN are efficiently migrating to the Ni_2P particles and act as N_2 reduction sites.[88] Decoration of BCN with Ag nanoparticles was found to enhance the activity by Yao et al.[86]

Wang et al. prepared S-doped C_3N_4 nanosheets from melamine and trithiocyanuric acid and used the resulting materials for photoconversion of nitrogen. This synthesis introduced carbon vacancies, which improved the adsorption and activation of N_2 molecules.[89] Hirai et al. comparably prepared P-doped C_3N_4 with nitrogen vacancies.[90]

Many groups employ g-C_3N_4 for the construction of semiconductor heterojunctions, e.g. heterojunctions of g-C_3N_4 and Cs_xWO_3 have been fabricated.[91] A Z-scheme like heterojunction photocatalyst has been constructed of Ga_2O_3 and g-C_3N_4 for nitrogen conversion, using alcohols as scavengers.[92] Wang et al. prepared an $LnCO_3OH$/g-C_3N_4 heterojunction to photoreduce dinitrogen. It showed high chemisorption for N_2, activating more N_2. Interestingly, a Z-scheme type of heterojunction without mediator was reported, separating the photoexcited charge carriers efficiently.[93]

Apart from oxides, sulfides such as ZnMoCdS have also been combined with g-C_3N_4.[94] Moreover, multiphase heterojunctions of $Zn_{0.8}Cd_{0.2}S$ with wurtzite and zincblende phases have been reported for photocatalytic nitrogen conversion.[58]

In summary, catalysts for which very high yields were observed, commonly include high concentrations of defects. Surface defects therefore seem to play a superior role in the improvement of photocatalytic nitrogen fixation as compared to the introduction of cocatalysts or the formation of hetero-

junctions. The best results are obtained when the strategies of defect engineering and heterojunction formation are combined.[95]

2.3. Reaction Engineering: Photoreactors and Performance Parameters

A quantitative comparison of the performance of different materials for photocatalytic nitrogen conversion raises several challenges. Analytical quantification of reduced or oxidized products in very low concentrations is an important challenge, that can further be complicated when the origin of the converted nitrogen has to be proven.[96–98] Awareness for the analytical challenges arose recently, mainly driven by electrochemical nitrogen conversion, but reaction engineering aspects represent an even greater challenge. While most relevant chemical information are commonly presented in the publications, more technical aspects are often missing or not stated in sufficient detail. This especially holds for the light source. Apart from not reporting important information such as applied optical filters and incident irradiance and the photoreactor itself, information on the geometrical setup of the light source and the reactor are almost entirely missing.[99]

Reaction engineering aspects can have a significant impact on the apparent performance of the investigated materials. Figure 6 gives an overview of important experimental parameters that influence the observed activity of materials for N_2 reduction. Not only that the reaction conditions differ significantly across the literature, reported performance metrics differ as well. To analyze the current state of knowledge, performance as well as experimental data from current literature are compiled in Table 1. Comparison of the quantitative data is enabled by reporting performance metrics as given in the publications as well as converting them (if necessary) into the volume specific rate of NH_4^+ formation [Equation (5)]:

$$r_{NH_4^+} = \frac{n_{NH_4^+}}{V\,t} \quad \left[r_{NH_4^+}\right] = \frac{\mathrm{mol}}{\mathrm{m^3 s}} \tag{5}$$

With $n_{NH_4^+}$ being the amount of NH_4^+ formed, V being the volume of the reaction solution and t being the reaction time. For a better readability, $r_{NH_4^+}$ is reported in units of $\left[r_{NH_4^+}\right] = \mu\mathrm{mol\ L^{-1}h^{-1}}$. Comparison of mass-based performance

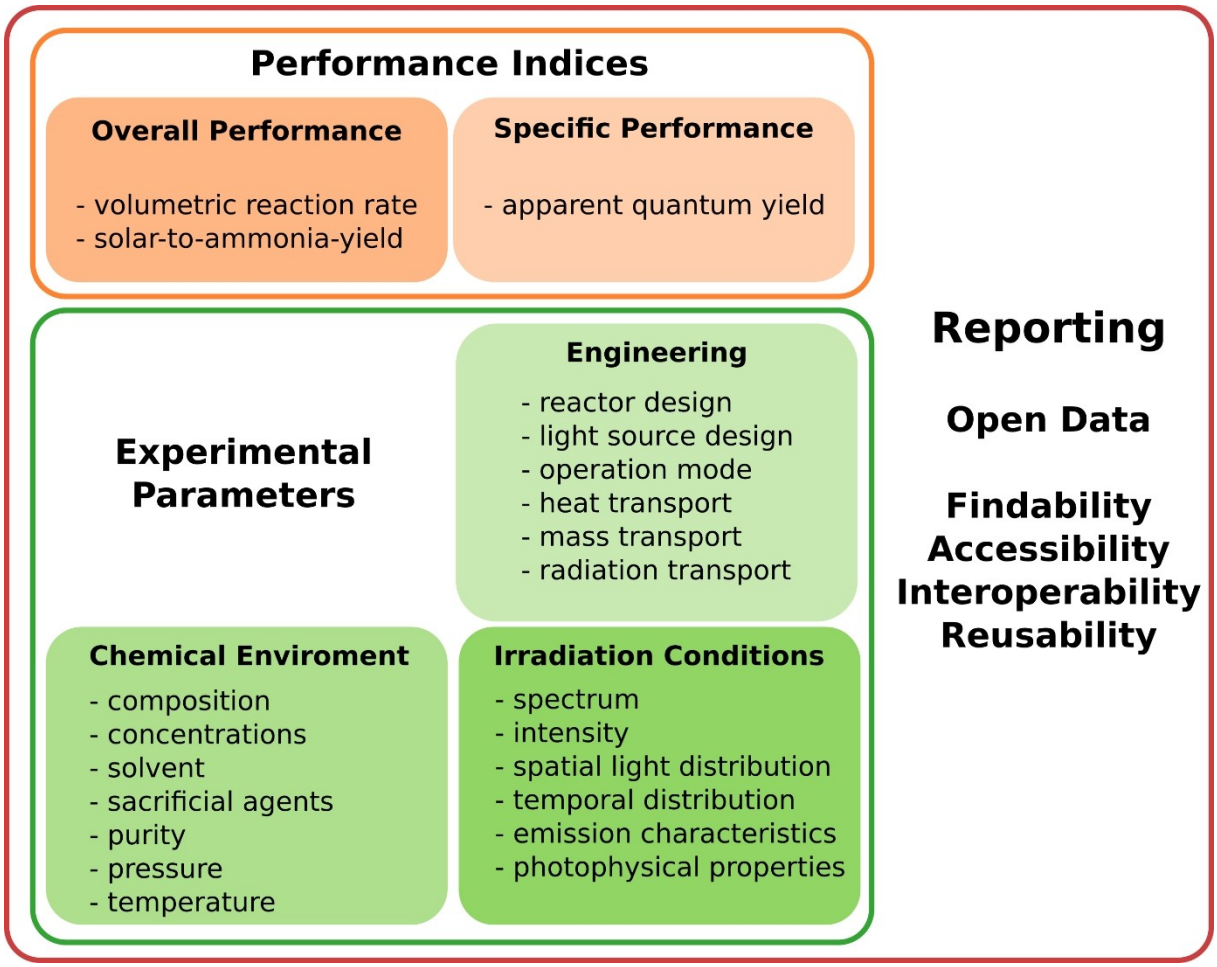

Figure 6. Important parameters that influence overall and specific performance indices. Comprehensive reporting following the FAIR principles is essential.[100]

Table 1. Reaction conditions and reported performance of reviewed publications. Information is reported as stated in the publications. Abbreviations are used as follows: NR: Nessler reagent; IC: ion chromatography; IP: indophenol blue indicator method; AA: Ammonia Assay (ab83360; Abcam; UK); LDH: layered double hydroxide; hp-Na: high pressure sodium lamp; Xe: Xenon arc lamp; hp-Hg: high pressure mercury lamp; DL: diode laser; Hg: unspecified mercury lamp; LED: light emitting diode; IR: infrared; conti: gas continuously bubbled through reaction solution; dis: gas dissolved prior to experiment; ?: specification unclear in publication; –: information not given in publication; RT: room temperature; sim sun: simulated sun light. Notes: [a] manufacturer information were unified and completed where possible: PLS-SE 300 or PLS-SE300 C/D/UV: PLS-SE 300 or PLS-SE300C/D/UV, Beijing Perfect Light Co., Ltd., China or Trusttech PLS-SE 300, Beijing, China; CEL-HF 300: CEL-HF 300, CeauLight Co., Ltd.; Solaredge 700 or Solaredge 300C: Solaredge 700/300C Perfect Light Company, China; CEL-S500: CEL-S500, Beijing China Education Au-light Co., Ltd.; LPF775A & SPF800A: LPF775A and SPF800A, Rayan Technology Co., Ltd.; PD-143: PD-143, China; Newport: Newport Corporation – Irvine, CA; Merc-500: NbeT, Merc-500. [b] unit stated in publication most likely wrong. [c] Filter solutions are stated with the used concentration of the used salt. Wavelengths are given in nm.

Reference	Year	Base Material	Best Activity	Activity Unit	r_{NH4+} [$\mu mol\,L^{-1}\,h^{-1}$]	AQE [%]	λ_{AQE} [nm]	SAY/ [%]	N_2 Source	Analytic Method	Temperature [°C]	Volume [mL]	Catalyst Amount	Catalyst Amount Unit	Light Source Type	Power [W]	Light Source Manufacturer[a]	Irradiance [mW cm^{-2}]	Spectrum[c]	Solvent
[109]	2017	$(BiO)_2CO_3$	38.2	$\mu mol\,h^{-1}\,g^{-1}$	0.8	–	–	0.006	N_2 conti	IP	RT	20	20	mg	Xe	300	–	100	sim sun	H_2O
[61]	2017	CuCr-LDH	184.8	$\mu mol\,L^{-1}\,h^{-1}$	184.8	0.44	380	–	N_2 dis	NR	25	20	50	mg	Xe	300	PLS-SE 300	–	200–800	H_2O
[110]	2018	Bi_2WO_6	160	$\mu mol\,h^{-1}\,g^{-1}$	8.0	–	–	–	N_2 conti	IP	20	100	0.1	g	Xe	300	PLS-SE 300	–	>420	H_2O
[63]	2018	BiOBr	75	$\mu mol\,L^{-1}\,h^{-1}$	75.0	2.1	380	–	N_2 dis	NR	RT	100	0	g	Xe	300	PLS-SE 300	–	AM 1.5 G	H_2O
[93]	2018	C_3N_4	8.91	$mmol\,L^{-1}\,h^{-1}\,g^{-1}$	267.3	–	–	–	Air dis?	NR	–	50	30	mg	Xe	500	–	–	sim sun	10 vol% CH_3OH/ H_2O
[111]	2018	C_3N_4	331	$\mu mol\,h^{-1}\,g^{-1}$	6.6	1.11	365	–	N_2 dis	NR	–	40	20	mg	LED	–	–	100	365–940	10 vol% CH_3OH/ H_2O
[112]	2018	C_3N_4	355.5	$\mu mol\,L^{-1}\,h^{-1}$	355.5	–	–	–	N_2 dis	NR	RT	50	0.1	g	0	100	–	346,000[b]	–	20 vol% C_2H_5OH/ H_2O
[113]	2018	C_3N_4	250.6	$\mu mol\,h^{-1}\,g^{-1}$	12.5	0.14	420	–	N_2 conti	NR	–	100	50	mg	Xe	300	CEL-HF 300	–	>420	20 vol% CH_3OH/ H_2O
[89]	2018	C_3N_4	5.99	$mmol\,L^{-1}\,h\text{-}1\,g^{-1}$	119.8	–	–	–	N_2 dis	NR	–	50	20	mg	Xe	500	–	–	AM 1.5 G	4 vol% C_2H_5OH/ H_2O
[80]	2018	C_3N_4	3.632	$mmol\,h^{-1}\,g^{-1}$	72.6	21.5	420	–	N_2 dis	NR	25	150	20	mg	Xe	300	–	–	AM 1.5 G	CH_3OH
[90]	2018	C_3N_4	0.2	$\mu mol\,h^{-1}$	0.2	0.95	420	0.1	N_2 conti	UV/vis/ IC	303	100	200	mg	Xe	2000	USHIO Inc.	40.7	>420	H_2O
[114]	2018	c-ZnO	245.7	$\mu mol\,L^{-1}\,h^{-1}\,g^{-1}$	24.6	–	–	–	N_2 dis	NR	–	200	0.1	g	Xe	300	–	–	>420	5 vol% C_2H_5OH/ H_2O
[26]	2018	$W_{18}O_{49}$	195.5	$\mu mol\,h^{-1}\,g^{-1}$	2.0	0.33	400	0.028	N_2 dis	NR	RT	10	10	mg	Xe	300	Solaredge 700	200	–	1 mM Na_2SO_3
[115]	2019	Attapulgite	157.29	$\mu mol\,L^{-1}\,h^{-1}$	157.3	–	–	–	N_2 conti	NR	–	100	0	g	Xe	300	–	–	sim sun	0.1 vol% C_2H_5OH/ H_2O
[48]	2019	Au	25.6	$\mu mol\,h^{-1}\,g^{-1}$	0.0	–	–	–	N_2 conti	IP	–	1	1.3	mg	Xe	500	CEL–S500	100	AM 1.5 G	20 vol% CH_3OH/ H_2O
[48]	2019	Au	114.3	$\mu mol\,h^{-1}\,g^{-1}$	0.1	–	–	–	N_2 conti	IP	56	1	1.3	mg	DL	1.6	–	8,000	808	20 vol% CH_3OH/ H_2O
[116]	2019	Bi_2O_3	1.7	$\mu mol\,L^{-1}\,h^{-1}$	1.7	–	–	–	N_2 conti	NR	RT	200	0.2	g	Xe	400	–	–	>400	H_2O
[60]	2019	$Bi_3FeMo_2O_{12}$	160.32	$\mu mol\,h^{-1}\,g^{-1}$	8.0	–	–	–	N_2 conti	IP	–	100	50	mg	hp-Hg	450	–	–	–	H_2O
[117]	2019	$Bi_4O_5Br_2$	327.3	$\mu mol\,L^{-1}\,h^{-1}\,g^{-1}$	16.4	–	–	–	N_2 conti	IP	–	50	50	mg	Xe	300	–	500	200–800	H_2O
[118]	2019	BiOBr	90.7	$\mu mol\,h^{-1}\,g^{-1}$	2.7	–	–	–	N_2 conti	NR	25	60	30	mg	Xe	300	–	–	–	H_2O
[66]	2019	BiOCl	63	$\mu mol\,L^{-1}\,h^{-1}$	63.0	–	–	–	N_2 dis	NR	RT	100	0.1	g	Xe	300	PLS-SE 300	–	>400	H_2O
[78]	2019	C_3N_4	5.5	$mg\,L^{-1}\,h^{-1}\,g^{-1}$	30.5	–	–	–	0.5 O_2, 0.5 N_2 conti	NR	–	500	0.1	g	hp-Na	250	–	–	400–800; 0.5 M $NaNO_2$	0.04 vol % CH_3OH/ H_2O
[119]	2019	C_3N_4	11	$mg\,L^{-1}\,h^{-1}\,g^{-1}$	61.0	–	–	–	N_2 dis	NR	–	500	0.1	g	hp-Na	250	–	–	400–800: 0.5 M $NaNO_2$	0.04 vol % CH_3OH/ H_2O
[30]	2019	C_3N_4	14	$mg\,L^{-1}\,h^{-1}\,g^{-1}$	77.6	–	–	–	N_2/O_2 conti	NR	–	500	0.1	g	IR + Xe	200 + 300	LPF775 A & SPF800 A	–	<800	0.04 vol % CH_3OH/ H_2O
[120]	2019	C_3N_4	214.6	$\mu mol\,L^{-1}\,h^{-1}$	214.6	–	–	0.046	N_2 dis	NR	RT	100	300	mg	Xe	300	PD-143	–	sim sun	20 vol% C_2H_5OH/ H_2O
[81]	2019	C_3N_4	3.42	$mmol\,h^{-1}\,g^{-1}$	34.2	–	–	–	N_2 dis	NR	RT	40	10	mg	Xe	300	CEL-HF 300	1000	>400	ethylene glycol
[82]	2019	C_3N_4	32.4	$\mu mol\,L^{-1}\,h^{-1}$	32.4	–	–	–	N_2 dis	NR	RT	100	50	mg	Xe	300	–	–	–	H_2O
[72]	2019	CdS	1	$mg\,L^{-1}\,h^{-1}$	55.4	0.75	420	–	N_2 conti	NR	25	100	100	mg	Xe	300	Solaredge 300 C	–	>420	H_2O
[121]	2019	d-Bi_2O_3	606	$\mu mol\,h^{-1}\,g^{-1}$	121.2	–	–	–	N_2 conti	NR	RT	200	0.2	g	Xe	400	–	–	>400	H_2O
[122]	2019	Graphene Oxide	130.3	$\mu mol\,L^{-1}\,h^{-1}$	130.3	–	–	0.028	N_2 dis	NR	RT	100	150	mg	Xe	300	PD-143	–	sim sun	H_2O

Table 1. continued

Reference	Year	Base Material	Best Activity	Activity Unit	r_{NH4+} [$\mu mol\,L^{-1}\,h^{-1}$]	AQE [%]	λ_{AQE} [nm]	SAY/ [%]	N_2 Source	Analytic Method	Temperature [°C]	Volume [mL]	Catalyst Amount	Catalyst Amount Unit	Light Source Type	Power [W]	Light Source Manufacturer[a]	Irradiance [mW cm^{-2}]	Spectrum[c]	Solvent
[73]	2019	Graphene Oxide	151.8	$\mu mol\,L^{-1}\,h^{-1}\,g^{-1}$	7.6	–	–	–	N_2 dis	IP	–	100	0.1	g	Xe	250	–	–	> UV	H_2O
[123]	2019	Graphene Oxide	409.4	$\mu mol\,L^{-1}\,h^{-1}\,g^{-1}$	20.5	–	–	–	N_2 dis	IP	–	100	50	mg	Xe	250	–	–	> UV	H_2O
[124]	2019	In_2O_3	40.1	$\mu mol\,h^{-1}\,g^{-1}$	0.8	–	–	–	N_2 conti	NR	15	100	0	g	Xe	300	–	200,000[b]	–	H_2O
[125]	2019	MOF-76(Ce)	34	$\mu mol\,h^{-1}\,g^{-1}$	1.7	–	–	–	N_2 dis	IP	–	100	50	mg	Xe	300	PLS-SE 300	–	–	H_2O
[52]	2019	MoO_3	11.1	$\mu mol\,L^{-1}\,h^{-1}\,g^{-1}$	0.6	0.01	365	–	N_2 conti	IC	25	100	50	mg	Xe	300	CEL-HF 300	–	300 – 2500	H_2O
[67]	2019	SmOCl	426	$\mu mol\,h^{-1}\,g^{-1}$	4.3	0.32	420	–	N_2 dis	NR/IC	–	20	10	mg	Xe	–	PLS–SE 300	–	–	H_2O
[59]	2019	$SrMoO_4$	93.1	$\mu mol\,L^{-1}\,h^{-1}\,g^{-1}$	5.6	–	–	–	N_2 conti	IP/NR	15	60	60	mg	Xe	300	–	–	–	H_2O
[56]	2019	$SrTiO_3$	30.1	$\mu mol\,h^{-1}\,g^{-1}$	0.5	–	–	–	N_2 dis	NR	25	150	15	mg	Xe	300	–	–	–	H_2O
[44]	2019	TiO_2	56.3	$\mu g\,h^{-1}\,g^{-1}$	0.1	–	–	–	N_2 conti	IP	25	100	40	mg	Xe	300	PLS-SE 300	1,438	–	20 vol% C_2H_5OH/ H_2O
[126]	2019	TiO_2	20.8	$\mu mol\,h^{-1}\,g^{-1}$	0.0	–	–	–	N_2 conti	IP	–	5	0	0	Xe	300	–	–	>420	20 vol% CH_3OH/ H_2O
[47]	2019	TiO_2	0.29	$mmol\,h^{-1}\,g^{-1}$	1.5	0.62	550	–	N_2 conti	NR/IP	20	50	5	mg	Xe	300	CEL–S500	100	>400	H_2O
[46]	2019	TiO_2	1.3	$\mu mol\,L^{-1}\,h^{-1}\,g^{-1}$	0.4	–	–	–	N_2 dis	IC	28	300	300	mg	Xe/Hg	300	Newport	–	320–IR	H_2O
[51]	2019	WO_3	230	$\mu mol\,h^{-1}\,g^{-1}$	2.3	–	–	–	–	NR	25	20	10	mg	Xe	–	PLS-SE 300	250	–	H_2O
[127]	2020	covalent triazine framework	171.4	$\mu mol\,h^{-1}\,g^{-1}$	8.6	–	–	–	N_2 dis	NR	RT	100	50	mg	Xe	300	–	–	420–780	H_2O
[103]	2020	Attapulgite	13.7	$mg\,L^{-1}\,h^{-1}$	761.3	–	–	–	N_2 dis	NR	30	100	0.1	g	Xe	300	–	–	>420	Na_2SO_3 solution
[128]	2020	Bi_2WO_6	30	$\mu mol\,h^{-1}\,g^{-1}$	4.5	–	–	–	N_2 dis	NR/IP/IC	RT	150	150	mg	Xe	–	PLS-SE 300D	400	>420	H_2O
[129]	2020	$BiFeO_3$	117.77	$\mu mol\,h^{-1}\,g^{-1}$	2.4	0.02	?	–	N_2 dis	IP	–	50	20	mg	Hg	250	–	95	>400	H_2O
[64]	2020	BiOBr	382.68	$\mu mol\,h^{-1}\,g^{-1}$	19.1	–	–	–	N_2 conti	AA	25	100	50	mg	Xe	300	–	–	>420	H_2O
[130]	2020	black phosporous	2.37	$mmol\,h^{-1}\,g^{-1}$	1.2	–	–	–	N_2 dis	NR	–	0	0.5	mg	LED	–	–	–	420	Na_2SO_3, Na_2S, H_2O
[131]	2020	C_3N_4	1090.33	$\mu mol\,L^{-1}\,h^{-1}\,g^{-1}$	43.6	–	–	–	N_2 dis?	NR	–	40	0	g	Xe	500	–	100	>420	0.1 vol% C_2H_5OH/ H_2O
[132]	2020	C_3N_4	4554	$\mu mol\,L^{-1}\,h^{-1}\,g^{-1}$	182.2	–	–	–	N_2 dis	NR	25	4	0	g	Xe	500	Ushio Inc.	100	>420	10 vol% C_2H_5OH/ H_2O
[79]	2020	C_3N_4	118.8	$mg\,L^{-1}\,h^{-1}\,g^{-1}$	65.9	5.28	–	–	N_2 conti	NR	25	50	10	mg	Xe	500	–	–	>420	10 vol% CH_3OH/ H_2O
[85]	2020	C_3N_4	0.44	$mmol\,h^{-1}\,g^{-1}$	11.0	1.28	400	0.042	N_2 dis	IP	RT	50	25	mg	Xe	300	PLS-SE 300D	200	AM 1.5 G	10 vol% CH_3OH/ H_2O
[133]	2020	C_3N_4	1118.5	$\mu mol\,L^{-1}\,h^{-1}\,g^{-1}$	44.7	–	–	–	Air dis	NR	25	2	0	g	Xe	500	–	100	>420	2 vol% C_2H_5OH/ H_2O
[87]	2020	C_3N_4	7.92	$mmol\,L^{-1}\,h\text{-}1\,g^{-1}$	198.0	–	–	–	N_2 dis	NR	–	100	25	mg	Xe	300	–	–	AM 1.5 G	20 vol% CH_3OH/ H_2O
[86]	2020	C_3N_4	5.19	$mg\,h^{-1}\,g^{-1}$	5.8	–	–	–	N_2 dis	NR	–	30	20	mg	Xe	300	PLS-SE 300D	–	–	5 vol% CH_3OH/ H_2O
[134]	2020	C_3N_4	442.92	$\mu g\,h^{-1}\,g^{-1}$	1.2	–	–	–	N_2 dis	IP	–	100	50	mg	Xe	300	PLS-SE 300/ PLS-SE 300UV	–	>400	diluted HCl
[88]	2020	C_3N_4	0.33	$\mu mol\,h^{-1}$	0.3	–	–	0.01	N_2 conti	IC	–	100	0.2	g	Xe	–	–	26,400[b]	>300	H_2O
[135]	2020	C_3N_4	122.67	$\mu mol\,h^{-1}\,g^{-1}$	6.1	–	–	–	N_2 dis	NR	25	100	50	mg	Xe	300	–	–	–	H_2O
[54]	2020	CeO_x	109	$\mu mol\,h^{-1}\,g^{-1}$	0.0	–	–	–	N_2 conti	IP	20	?	?	?	?	?	?	–	?	H_2O
[136]	2020	$Cu^{\delta+}$-Modified Defective ZnAl-LDH	110	$\mu mol\,h^{-1}\,g^{-1}$	0.6	1.77	265	0.014	N_2 dis	IC	25	100	5	mg	Xe	300	CEL-HF 300	5,100	200–800	H_2O
[137]	2020	$InVO_4$	626	$\mu mol\,h^{-1}\,g^{-1}$	12.5	–	–	–	N_2 dis	NR	RT	100	0	g	Xe	300	PLS-SE 300	–	–	H_2O
[138]	2020	$K_{11}[PMo_4V_8O_{40}]$	149	$\mu mol\,L^{-1}\,h^{-1}$	149.0	–	–	0.032	–	NR	RT	100	300	mg	Xe	300	PD-143	–	–	20 vol% C_2H_5OH/ H_2O
[139]	2020	$KNbO_3$	470.6	$\mu mol\,h^{-1}\,g^{-1}$	47.1	–	–	–	N_2 dis	NR	–	100	0.1	g	Xe	300	PLS-SE 300 C	–	–	10 vol% C_2H_5OH/ H_2O
[53]	2020	MoO_3	328	$\mu mol\,L^{-1}\,h^{-1}\,g^{-1}$	16.4	0.3	800	–	N_2 conti	NR	25	100	50	mg	Xe	300	–	–	–	H_2O

Table 1. continued

Reference	Year	Base Material	Best Activity	Activity Unit	r_{NH4+} [μmol L^{-1} h^{-1}]	AQE [%]	λ_{AQE} [nm]	SAY/ [%]	N_2 Source	Analytic Method	Temperature [°C]	Volume [mL]	Catalyst Amount	Catalyst Amount Unit	Light Source Type	Power [W]	Light Source Manufacturer[a]	Irradiance [mW cm^{-2}]	Spectrum[c]	Solvent
[71]	2020	MoS_2	820.83	μmol L^{-1} h^{-1} g^{-1}	164.4	4.44	AM 1.5 G	–	N_2 dis	NR	–	100	0	g	Xe	–	–	–	AM 1.5 G	20 vol% CH_3OH/ H_2O
[71]	2020	MoS_2	962.03	μmol L^{-1} h^{-1} g^{-1}	19.2	–	–	–	N_2 dis	NR	–	100	0	g	Xe	–	–	–	AM 1.5 G	H_2O
[140]	2020	Mxene	56.67	μmol L^{-1} h^{-1} g^{-1}	2.8	–	–	–	N_2 conti	IP	–	100	50	mg	Xe	–	–	100	–	H_2O
[141]	2020	NH_2-MIL-125 (Ti)	12.3	μmol h^{-1} g^{-1}	0.3	0.26	400	–	N_2 dis	IC	–	100	25	mg	Xe	300	–	–	>400	H_2O
[142]	2020	TiO_2	324.86	μmol h^{-1} g^{-1}	16.2	1.1	365	–	N_2 dis	IC	25	100	50	mg	Xe	300	–	–	–	10 vol% CH_3OH/ H_2O
[37]	2020	TiO_2	1.2	mmol L^{-1} h^{-1}	24.0	–	–	–	N_2 dis	NR	–	50	20	mg	Xe	300	–	–	–	5 vol% CH_3OH/ H_2O
[43]	2020	TiO_2	1.1	μmol h^{-1}	1.1	0.1	350	–	N_2 conti	IP	25	100	30	mg	hp-Hg	500	Merc-500	–	–	H_2O
[34]	2020	TiO_2	52.4	μmol L^{-1} h^{-1} g^{-1}	2.6	–	–	–	N_2 dis	IP/IC	RT	100	50	mg	Xe	300	CEL-WLA500	300	–	H_2O
[143]	2020	TiO_2	422	μmol h^{-1} g^{-1}	4.2	0.15	400	–	N_2 dis?	NR	RT	20	10	mg	Xe	–	–	250	320–780	H2O
[58]	2020	$Zn_{0.8}Cd_{0.2}S$	25	μmol h^{-1} g^{-1}	0.6	–	–	–	N_2 dis	IP	20	50	25	mg	Xe	–	PLS-SE 300 C	–	>420	H_2O
[41]	2021	TiO_2	206	μmol h^{-1} g^{-1}	103.0	0.38	420	–	N_2 dis	IC	27	500	0.5	g	Xe	300	–	–	–	H_2O

metrics should be avoided due to the following reasons.[101] First, the rate of photocatalytic reactions is not proportional to the catalyst mass.[102] Too high loadings can cause dark zones, not contributing to the overall performance. On the other side, very low catalyst loadings can lead to analytical issues when low amounts of NH_4^+ need to be quantified. Second, data that is scaled to the amount of photocatalyst can suggest very high performance, that is artificially amplified when using very low amounts of photocatalyst. From the reaction engineering perspective, such conditions are detrimental since either only a small share of the incident light is utilized (low optical density/ degree of absorption) or large optical lengths and with this, large reactors would be required.

A look on the reported volume specific rate of NH_4^+ formation reveals outstanding performance of metal oxides with maximum rates of 760 μmol L^{-1} h^{-1} (Figure 7). Carbon nitrides show formation rates of up to 355 μmol L^{-1} h^{-1}. Except for the attapulgite used in 2020,[103] the reported performance of new materials was either lower or stagnated as for previously reported materials. For carbon nitrides the trend even shows a decreasing performance. The only exception are metal sulfides on which only in 2019 and 2020 were reported and for which an increase is found. In general, the number of materials investigated for their activity for N_2 reduction increased strongly in 2019 and 2020.

When *excluding* all publications that used sacrificial agents, the absolute numbers decrease but the overall trends stay the same. The maximum reported NH_4^+ formation rate is 184 μmol L^{-1} h^{-1} for a CuCr-LDH reported in 2017.[61] For more recent years, reported performance stagnated. The highest reported formation rates for metal sulfides, carbon nitrides and hybrids were 55 μmol L^{-1} h^{-1}, 32 μmol L^{-1} h^{-1} and 9 μmol L^{-1} h^{-1}, respectively.

An analysis of the data gathered in Table 1 reveals the following general insights into the current activities on photocatalytic nitrogen activation. Photocatalytic activity is exclusively tested in batch reactors, with volumes of 1 to 500 mL. Temperature control is maintained in some of the published work, but at several points it is unclear how this is achieved since the used vessels lack the possibility for tempering. This point is of special relevance when high power light sources are utilized, which can heat up the reactor through the emitted IR radiation. In general, specific information on the used reactors are very sparse. Unsurprisingly, the preferred reaction temperature is 25 °C or "room temperature".

The research activities are mostly focusing on the use of solar light and consequently, xenon arc lamps are the most popular light sources, often equipped with filters. Except when photocatalytic activity is reported for irradiation with AM 1.5 G filters, comparison can be biased since information on the optical characteristics are seldom reported. To ensure comparability, the applied irradiance must be reported as well, which is only the case for less than one third of the publications gathered in the table. Even for publications stating the applied irradiance, the used intensities vary from about 100 to 26,400 mW cm^{-2}. Hence, results with incident photon fluxes varying by more than an order of magnitude need to be

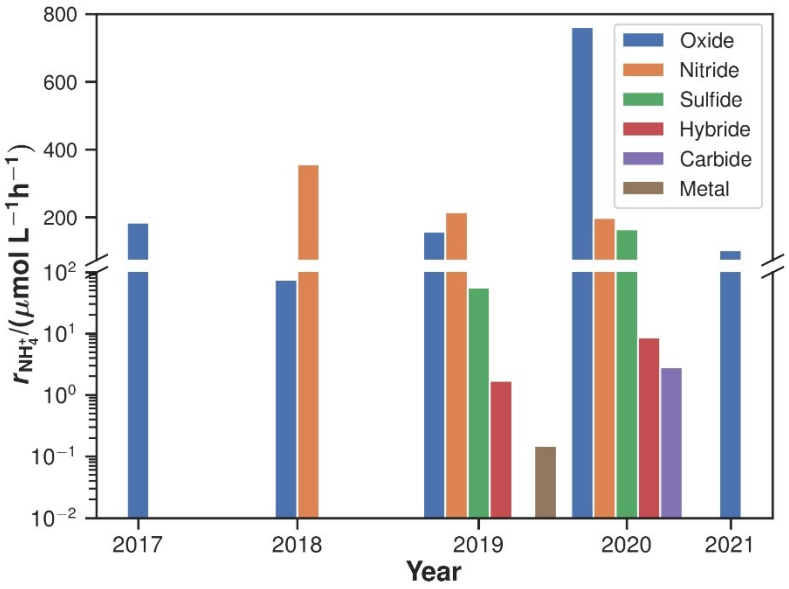

Figure 7. Maximum volumetric rate of NH_4^+ formation reported per year and material class.

compared. Due to the aging of Xe lamp, the actual light output of the used light source must be checked periodically and operating parameters must be adapted to ensure a constant irradiance throughout all experiments. With respect to comparability, reporting the absolute incident photon flux or the absolute incident radiation power would be advisable since these metrics implicitly consider the characteristics of the used experimental setup.[104] Actinometric and multidimensional radiometric measurements are well suited for these characterizations.[105,106] Even simple differences such as irradiation of a reactor from the bottom or the top have been shown to cause significant differences on the incident photon flux inside the reaction solution (>30%).[99] Aiming for a comparability of performance data, the use of solar simulators with a defined irradiance together with a reactor comprising an irradiation window of defined size are highly desirable. This would ensure that the absolute incident photon flux is the same for every experiment. It is worth mentioning that photocatalytic activity in the UV region is hardly investigated. For most reported data, the UV region is explicitly excluded. Usually, activities are higher – sometimes significantly – when UV light is included.

Independent of this activity measurement, investigations on the impact of other reaction parameters on the performance of the material are important. In this context, the chemical environment used to probe the photocatalytic activity needs additional consideration. From the presented data set, only about 50% of the reported materials were tested without using sacrificial agents. Since the addition of sacrificial agents was generally observed to improve the yield of ammonia,[29] this causes additional problems for a good comparability because not all groups employ the same scavengers at the same concentration. For example, the yields reported for KOH etched g-C_3N_4 are halved when the methanol concentration was lowered to 20%.[80] It is well possible that photocatalysts whose yields are relatively low, but which are based on the same material class, might show higher activity under different conditions.

Despite the issues with comparability reported above, some insights can be gained from analysis of performance data. Several publications report on the solar-to-ammonia-yield (SAY), which can beneficially be used for comparison since the irradiation conditions are defined by the AM 1.5 G spectrum with an irradiance of 100 mW cm^{-2}.[107] The SAY can be calculated with Equations (6), (7):

$$SAY = \frac{\Delta G\ for\ NH_3\ formation \times\ NH_3\ formed}{total\ incident\ energy \times\ reaction\ time} \quad (6)$$

$$[SAY] = 1 = \frac{J}{mol} \times mol \times \frac{s}{J} \times \frac{1}{s} \quad (7)$$

with $\Delta G_{NH_3} = 339$ kJ mol^{-1}.[108] The total energy input has to be calculated from the AM 1.5 G irradiance of 100 mW cm^{-2} and the irradiated area of the used experimental setup. Figure 8 shows the performance data for different types of materials and year. While only about 10% of the publications calculate this performance metric, it is obvious that little progress has been made with respect to the SAY. Converting 0.1% of the solar irradiation to ammonia is the highest yield that could be obtained for photocatalytic nitrogen conversion till now. In general, nitrides show a higher efficiency as oxides, but no progress in increasing the SAY has been reported during the last 3 years for nitrides. The efficiency of oxides has slightly increased from 0.006% to 0.032% since 2017. Compared to water splitting, converting nitrogen photocatalytically is currently one order of magnitude less efficient.[19]

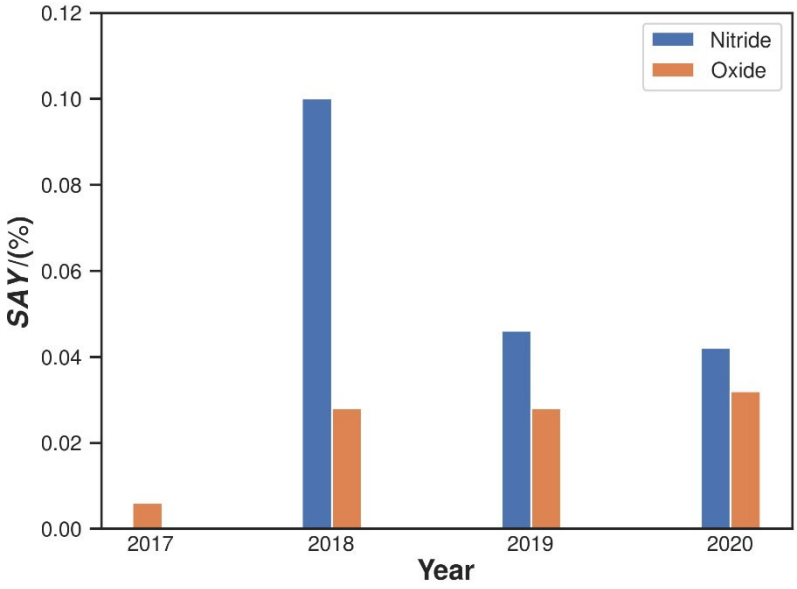

Figure 8. Maximum SAY reported per year and material class.

The apparent quantum yield/efficiency (AQY/AQE) is well suited to quantify the performance of the materials as well [Equations (8), (9)].

$$AQY = \frac{NH_3\ formed \times 3}{total\ amount\ of\ incident\ photons} \tag{8}$$

$$[AQY] = 1 = \frac{mol}{mol} \tag{9}$$

Normalization to the incident photon flux (in the photoreactor) rules out the impact of the experimental setup. The data compiled in Figure 9 show that the overall efficiency of converting photons to ammonia for most materials is still low, not surpassing 2.5%. The maximum efficiency of oxide materials was found to be higher than that of other material classes, except for one carbon nitride material with an outstanding AQE of 21.5%. Again, no significant increase of the AQY was demonstrated in recent years.

3. Conclusions

From the literature survey it becomes obvious that current research efforts lack a systematic approach that ensures comparability between the various material approaches that

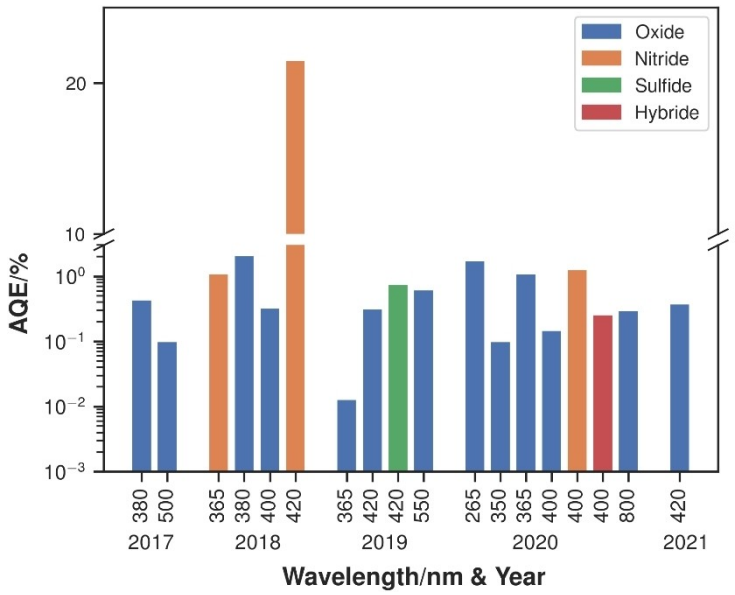

Figure 9. Maximum AQY reported per year, material class and wavelength.

are used for photocatalytic N_2 conversion. To overcome this limitation, future research efforts and especially publications must pay special attention to the reproducibility and documentation of the experiments to allow for more quantitative approaches.[144] The potentials of the open data approaches must be considered through e.g. the four FAIR principles, namely Findability, Accessibility, Interoperability, and Reusability.[100] This is of particular importance for the reaction engineering aspects of photocatalyst development. Performance characterization for solar irradiation conditions is a first step to realize comparability, given that sacrificial donors are relinquished. This standardization approach needs to be extended by well documented efforts to optimize the photocatalytic activity with respect to reaction engineering aspects such as irradiation conditions, chemical environment or reactor concepts. The large variety of different materials and with this physical and chemical material properties require a thorough optimization of the reaction conditions to unleash the full potential of the material under investigation and gain understanding for further material optimization. The tools to realize the required comparability are now available but need to be used across the whole community to increase general understanding and allow for a cross fertilization of knowledge for the different material types.

Besides the challenges of well documented experimental data, reaction engineering aspects are completely unexplored and methodological understanding of the impact on photocatalytic nitrogen conversion is missing. Current research uses mainly simple lab reactors to investigate the performance of different photocatalysts, in which nitrogen is converted that is either dissolved prior to the experiments or bubbled through the liquid reaction solution during irradiation. The temporal evolution of the reaction conditions is completely different for both approaches: the concentration of N_2 decreases with time for the first, discontinuous approach, while it is more constant for the second, semicontinuous approach. The impact of this effect is currently unclear for the reported catalytic systems, but general knowledge on solubility of N_2, mass transport effects and reaction kinetics of catalysis suggest that more attention needs to be paid to this aspect. For instance, for homogeneous water splitting systems, switching from discontinuous to semicontinuous operation resulted in a dramatic drop of activity.[145] As already outlined above, the emission characteristics of light sources, the design of the reactor and the absorption and scattering characteristics of the photocatalysts further impact the apparent activity. The importance of this aspect becomes clear when considering the vision of using natural solar irradiation to drive complete chemical plants for N_2 conversion. The fluctuating nature of solar radiation causes unsteady reaction conditions that need to be considered during reactor as well as material development.[146] Hence, systematic research at the interface between material development and chemical engineering is highly desirable for the future development of highly performant and efficient photocatalytic processes for N_2 conversion. Because of the interaction of material properties, reaction environment and activity, joint research right from the beginning is key for a fast progress in this research field by leveraging the synergies between both disciplines.

Considering the materials aspects for N_2 reduction, and comparing the state of research of the field to the water splitting community about twenty years ago, it is easy to see that hardly any nitrogen reduction with UV light-absorbing materials is investigated. This was different for water splitting, when many different mixed metal oxides were found to split water,[147] some of them with very high apparent quantum yields.[148] This period was very important for the water splitting research, for a knowledge-based improvement of materials, compositions, and surface decorations or reconstructions. In today's N_2 reduction research, the impression arises that mainly the "usual suspects" materials are investigated for the reaction, instead of considering the high performance water splitting systems for N_2 reduction. Besides the selectivity problem, which has to be dealt with in the future, N_2 reduction yields and solar-to-ammonia yields are extremely low, thus such materials might be worth checking: Water splitting has outgrown its infancy, quantum yields of nearly unity are achieved by much improved charge carrier separation,[149] and solar-to-hydrogen efficiencies above 1% are possible.[150] This might be a starting point for a more focused materials development for photocatalytic N_2 conversion. These activities must be accompanied by research on the selectivity aspects for which electrocatalytic N_2 reduction already offers valuable insights.[151] Moreover, it can hardly be overseen that no reaction engineering aspects are considered so far in N_2 reduction. While in CO_2 reduction this aspect has drawn a lot of attention early, due to false results coming from carbon impurities, this must be addressed immediately in N_2 reduction to ensure comparable experimental data as well a synergistic materials development. It has been considered already in the electrocatalytic field,[20,152] but needs to be accepted in the photocatalytic area as well. The influence of N_2 supply, pressure, temperature, solvent, mode of operation and especially reactor design have to be considered together with the molecular reaction and material considerations.

Finally, the use of sacrificial agents needs to be reduced. Yes, reducing nitrogen in water/methanol could still be called nitrogen reduction (different to the term of water splitting often falsely used for hydrogen production from water/methanol[153]), but what is it worth for? Except for one example, almost no progress for N_2 reduction in pure water as well as in sacrificial agent systems during the last 3 years has been reported.

Until now, most research efforts did not consider the requirement of a joint interdisciplinary effort. Hence, progress is only made in single disciplines without acknowledging synergies. We believe that only in a joint effort with strong interactions between chemists, physicists and chemical engineers already on the fundamental level, a fast development and the establishment of applicable material and reactor systems for photocatalytic N_2 reduction will become possible. With such an obtained joint fundamental knowledge on

material design, process and reaction engineering, a knowledge transfer of the gained understanding to application might be possible.

Acknowledgements

Open access funding enabled and organized by Projekt DEAL.

Conflict of Interest

The authors declare no conflict of interest.

Keywords: heterojunctions · nitrogen reduction · photocatalysis · reaction engineering · semiconductors

[1] J. W. Erisman, M. A. Sutton, J. Galloway, Z. Klimont, W. Winiwarter, *Nat. Geosci.* **2008**, *1*, 636–639.
[2] K. H. R. Rouwenhorst, P. M. Krzywda, N. E. Benes, G. Mul, L. Lefferts, *Ammonia, 4. Green ammonia Production, in Ullmann's Encycl. Ind. Chem.*, Wiley, **2020**, pp. 1–20.
[3] M. Appl, in *Ullmann's Encycl. Ind. Chem.*, Wiley-VCH Verlag GmbH & Co. KGaA, Weinheim, Germany, **2011**.
[4] L. Wang, M. Xia, H. Wang, K. Huang, C. Qian, C. T. Maravelias, G. A. Ozin, *Joule* **2018**, *2*, 1055–1074.
[5] Z. Du, D. Denkenberger, J. M. Pearce, *Sol. Energy* **2015**, *122*, 562–568.
[6] B. M. Hoffman, D. Lukoyanov, Z.-Y. Yang, D. R. Dean, L. C. Seefeldt, *Chem. Rev.* **2014**, *114*, 4041–4062.
[7] J. G. Chen, R. M. Crooks, L. C. Seefeldt, K. L. Bren, R. M. Bullock, M. Y. Darensbourg, P. L. Holland, B. Hoffman, M. J. Janik, A. K. Jones, M. G. Kanatzidis, P. King, K. M. Lancaster, S. V. Lymar, P. Pfromm, W. F. Schneider, R. R. Schrock, *Science* **2018**, *360*, eaar6611.
[8] K. A. Brown, D. F. Harris, M. B. Wilker, A. Rasmussen, N. Khadka, H. Hamby, S. Keable, G. Dukovic, J. W. Peters, L. C. Seefeldt, P. W. King, *Science* **2016**, *352*, 448–450.
[9] X.-Y. Xie, P. Xiao, W.-H. Fang, G. Cui, W. Thiel, *ACS Catal.* **2019**, *9*, 9178–9187.
[10] M. D. Fryzuk, S. A. Johnson, *Coord. Chem. Rev.* **2000**, *200–202*, 379–409.
[11] A. J. Medford, M. C. Hatzell, *ACS Catal.* **2017**, *7*, 2624–2643.
[12] N. R. Dhar, N. N. Pant, *Nature* **1944**, *3873*, 115–116.
[13] S. G. Bratsch, *J. Phys. Chem. Ref. Data* **1989**, *18*, 1–21..
[14] G. N. Schrauzer, T. D. Guth, *J. Am. Chem. Soc.* **1977**, *99*, 7189–7193.
[15] X. Chen, N. Li, Z. Kong, W.-J. Ong, X. Zhao, *Mater. Horiz.* **2018**, *5*, 9–27.
[16] C. J. M. van der Ham, M. T. M. Koper, D. G. H. Hetterscheid, *Chem. Soc. Rev.* **2014**, *43*, 5183–5191.
[17] Y. Xin, S. Wang, H. Yuan, T. Hou, W. Zhu, Y. Liu, Y. Yao, W. Zhang, S. Liang, L. Wang, *Chem* **2021**, DOI 10.1016/j.chempr.2021.03.018.
[18] J. Choi, B. H. R. Suryanto, D. Wang, H. L. Du, R. Y. Hodgetts, F. M. Ferrero Vallana, D. R. MacFarlane, A. N. Simonov, *Nat. Commun.* **2020**, *11*, 5546.
[19] J. H. Kim, D. Hansora, P. Sharma, J.-W. Jang, J. S. Lee, *Chem. Soc. Rev.* **2019**, *48*, 1908–1971.
[20] B. H. R. Suryanto, H.-L. Du, D. Wang, J. Chen, A. N. Simonov, D. R. MacFarlane, *Nat. Catal.* **2019**, *2*, 290–296.
[21] B. M. Comer, P. Fuentes, C. O. Dimkpa, Y.-H. Liu, C. A. Fernandez, P. Arora, M. Realff, U. Singh, M. C. Hatzell, A. J. Medford, *Joule* **2019**, *3*, 1578–1605.
[22] S. Zhang, Y. Zhao, R. Shi, G. I. N. Waterhouse, T. Zhang, *EnergyChem* **2019**, *1*, 100013.
[23] M. Cheng, C. Xiao, Y. Xie, *J. Mater. Chem. A* **2019**, *7*, 19616–19633.
[24] R. Shi, Y. Zhao, G. I. N. Waterhouse, S. Zhang, T. Zhang, *ACS Catal.* **2019**, *9*, 9739–9750.
[25] J. Yang, Y. Guo, R. Jiang, F. Qin, H. Zhang, W. Lu, J. Wang, J. C. Yu, *J. Am. Chem. Soc.* **2018**, *140*, 8497–8508.
[26] N. Zhang, A. Jalil, D. Wu, S. Chen, Y. Liu, C. Gao, W. Ye, Z. Qi, H. Ju, C. Wang, X. Wu, L. Song, J. Zhu, Y. Xiong, *J. Am. Chem. Soc.* **2018**, *140*, 9434–9443.
[27] S. Hu, X. Chen, Q. Li, F. Li, Z. Fan, H. Wang, Y. Wang, B. Zheng, G. Wu, *Appl. Catal. B* **2017**, *201*, 58–69.
[28] N. Tong, Y. Wang, Y. Liu, M. Li, Z. Zhang, H. Huang, T. Sun, J. Yang, F. Li, X. Wang, *J. Catal.* **2018**, *361*, 303–312.
[29] L. Ye, C. Han, Z. Ma, Y. Leng, J. Li, X. Ji, D. Bi, H. Xie, Z. Huang, *Chem. Eng. J.* **2017**, *307*, 311–318.
[30] H. Liang, L. Fang, S. Hu, *New J. Chem.* **2019**, *43*, 12094–12102.
[31] Y. Wang, W. Wei, M. Li, S. Hu, J. Zhang, R. Feng, *RSC Adv.* **2017**, *7*, 18099–18107.
[32] J. Soria, J. C. Conesa, V. Augugliaro, L. Palmisano, M. Schiavello, A. Sclafani, *J. Phys. Chem.* **1991**, *95*, 274–282.
[33] H. Hirakawa, M. Hashimoto, Y. Shiraishi, T. Hirai, *J. Am. Chem. Soc.* **2017**, *139*, 10929–10936.
[34] Y. Liao, J. Lin, B. Cui, G. Xie, S. Hu, *J. Photochem. Photobiol. A* **2020**, *387*, 112100.
[35] S. Wu, X. Tan, K. Liu, J. Lei, L. Wang, J. Zhang, *Catal. Today* **2019**, *335*, 214–220.
[36] G. Zhang, X. Yang, C. He, P. Zhang, H. Mi, *J. Mater. Chem. A* **2020**, *8*, 334–341.
[37] J. Wang, W. Lin, Y. Ran, J. Cui, L. Wang, X. Yu, Y. Zhang, *J. Phys. Chem. C* **2020**, *124*, 1253–1259.
[38] C. Li, T. Wang, Z.-J. Zhao, W. Yang, J.-F. Li, A. Li, Z. Yang, G. A. Ozin, J. Gong, *Angew. Chem. Int. Ed.* **2018**, *57*, 5278–5282; *Angew. Chem.* **2018**, *130*, 5376–5380.
[39] B. M. Comer, A. J. Medford, *ACS Sustainable Chem. Eng.* **2018**, *6*, 4648–4660.
[40] Y. Zhao, Y. Zhao, R. Shi, B. Wang, G. I. N. Waterhouse, L. Wu, C. Tung, T. Zhang, *Adv. Mater.* **2019**, *31*, 1806482.
[41] R. Guan, D. Wang, Y. Zhang, C. Liu, W. Xu, J. Wang, Z. Zhao, M. Feng, Q. Shang, Z. Sun, *Appl. Catal. B* **2021**, *282*, 119580.
[42] K. T. Ranjit, T. K. Varadarajan, B. Viswanathan, *J. Photochem. Photobiol. A* **1996**, *96*, 181–185.
[43] S. Chang, X. Xu, *Inorg. Chem. Front.* **2020**, *7*, 620–624.
[44] S. Liu, Y. Wang, S. Wang, M. You, S. Hong, T.-S. S. Wu, Y.-L. L. Soo, Z. Zhao, G. Jiang, J. Qiu, B. Wang, Z. Sun, Jieshan Qiu, B. Wang, Z. Sun, J. Qiu, B. Wang, Z. Sun, *ACS Sustainable Chem. Eng.* **2019**, *7*, 6813–6820.
[45] B. M. Comer, Y.-H. H. Liu, M. B. Dixit, K. B. Hatzell, Y. Ye, E. J. Crumlin, M. C. Hatzell, A. J. Medford, *J. Am. Chem. Soc.* **2018**, *140*, 15157–15160.
[46] Y.-H. Liu, M. H. Vu, J. Lim, T.-O. Do, M. C. Hatzell, *Faraday Discuss.* **2019**, *215*, 379–392.
[47] T.-A. A. Bu, Y.-C. C. Hao, W.-Y. Y. Gao, X. Su, L.-W. W. Chen, N. Zhang, A.-X. X. Yin, *Nanoscale* **2019**, *11*, 10072–10079.
[48] H. Jia, A. Du, H. Zhang, J. Yang, R. Jiang, J. Wang, C. Y. Zhang, *J. Am. Chem. Soc.* **2019**, *141*, 5083–5086.
[49] T. Oshikiri, X. Shi, H. Misawa, *Eur. J. Inorg. Chem.* **2020**, *2020*, 1396–1401.
[50] M.-H. Vu, C.-C. Nguyen, T.-O. Do, *ACS Sustainable Chem. Eng.* **2020**, *8*, 12321–12330.
[51] T. Hou, Y. Xiao, P. Cui, Y. Huang, X. Tan, X. Zheng, Y. Zou, C. Liu, W. Zhu, S. Liang, L. Wang, *Adv. Energy Mater.* **2019**, *9*, 1902319.
[52] Y. Li, X. Chen, M. Zhang, Y. Zhu, W. Ren, Z. Mei, M. Gu, F. Pan, *Catal. Sci. Technol.* **2019**, *9*, 803–810.
[53] H. Wu, X. Li, Y. Cheng, Y. Xiao, R. Li, Q. Wu, H. Lin, J. Xu, G. Wang, C. Lin, X. Chen, Y. Wang, *J. Mater. Chem. A* **2020**, *8*, 2827–2835.
[54] C. Zhang, Y. Xu, C. Lv, L. Bai, J. Liao, Y. Zhai, H. Zhang, G. Chen, *Appl. Catal. B* **2020**, *264*, 118416.
[55] Q. Li, K. Domen, S. Naito, T. Onishi, K. Tamaru, *Chem. Lett.* **1983**, *12*, 321–324.
[56] Z. Ying, S. Chen, T. Peng, R. Li, J. Zhang, *Eur. J. Inorg. Chem.* **2019**, *2019*, 2182–2192.
[57] Y. Hao, X. Dong, S. Zhai, H. Ma, X. Wang, X. Zhang, *Chem. A Eur. J.* **2016**, *22*, 18722–18728.
[58] W. Dong, Y. Liu, G. Zeng, T. Cai, L. Shao, H. Chen, W. Zeng, X. Xia, *J. Photochem. Photobiol. A* **2020**, *401*, 112766.
[59] J. Luo, X. Bai, Q. Li, X. Yu, C. Li, Z. Wang, W. Wu, Y. Liang, Z. Zhao, H. Liu, *Nano Energy* **2019**, *66*, 104187.
[60] B. Liu, A. S. Yasin, T. Musho, J. Bright, H. Tang, L. Huang, N. Wu, *J. Electrochem. Soc.* **2019**, *166*, H3091–H3096.
[61] Y. Y. Zhao, Y. Y. Zhao, G. I. N. N. Waterhouse, L. Zheng, X. Cao, F. Teng, L.-Z. Z. Wu, C.-H. H. Tung, D. O'Hare, T. Zhang, *Adv. Mater.* **2017**, *29*, 1703828.
[62] H. Li, J. Shang, Z. Ai, L. Zhang, *J. Am. Chem. Soc.* **2015**, *137*, 6393–6399.
[63] Y. Bi, Y. Wang, X. Dong, N. Zheng, H. Ma, X. Zhang, *RSC Adv.* **2018**, *8*, 21871–21878.
[64] Y. Liu, Z. Hu, J. C. Yu, *Chem. Mater.* **2020**, *32*, 1488–1494.

[65] H. Liu, Z. Fang, Y. Su, Y. Suo, S. Huang, Y. Zhang, K. Ding, *Chem. Asian J.* **2018**, *13*, 799–808.
[66] D. Wu, R. Wang, C. Yang, Y. An, H. Lu, H. Wang, K. Cao, Z. Gao, W. Zhang, F. Xu, K. Jiang, *J. Colloid Interface Sci.* **2019**, *556*, 111–119.
[67] T. Hou, R. Guo, L. Chen, Y. Xie, J. Guo, W. Zhang, X. Zheng, W. Zhu, X. Tan, L. Wang, *Nano Energy* **2019**, *65*, 104003.
[68] M. Lashgari, P. Zeinalkhani, *Appl. Catal. A* **2017**, *529*, 91–97.
[69] Q. Liu, L. Ai, J. Jiang, *J. Mater. Chem. A* **2018**, *6*, 4102–4110.
[70] S. Sun, X. Li, W. Wang, L. Zhang, X. Sun, *Appl. Catal. B* **2017**, *200*, 323–329.
[71] B. Sun, Z. Liang, Y. Qian, X. Xu, Y. Han, J. Tian, *ACS Appl. Mater. Interfaces* **2020**, *12*, 7257–7269.
[72] X. Gao, L. An, D. Qu, W. Jiang, Y. Chai, S. Sun, X. Liu, Z. Sun, *Sci. Bull.* **2019**, *64*, 918–925.
[73] S.-X. X. Wang, H. Maimaiti, B. Xu, A. Awati, G.-B. Bin Zhou, Y. dan Cui, *Appl. Surf. Sci.* **2019**, *493*, 514–524.
[74] P. Xing, P. Chen, Z. Chen, X. Hu, H. Lin, Y. Wu, L. Zhao, Y. He, *ACS Sustainable Chem. Eng.* **2018**, *6*, 14866–14879.
[75] K. Wang, D. Smith, Y. Zheng, *Carbon Resour. Convers.* **2018**, *1*, 2–31..
[76] G. Dong, W. Ho, C. Wang, *J. Mater. Chem. A* **2015**, *3*, 23435–23441.
[77] H. Ma, Z. Shi, Q. Li, S. Li, *J. Phys. Chem. Solids* **2016**, *99*, 51–58.
[78] Y. Zhao, E. Wang, R. Jin, *Diamond Relat. Mater.* **2019**, *94*, 146–154.
[79] T. Huang, S. Pan, L. Shi, A. Yu, X. Wang, Y. Fu, *Nanoscale* **2020**, *12*, 1833–1841.
[80] X. Li, X. Sun, L. Zhang, S. Sun, W. Wang, *J. Mater. Chem. A* **2018**, *6*, 3005–3011.
[81] W. Wang, H. Zhang, S. Zhang, Y. Liu, G. Wang, C. Sun, H. Zhao, *Angew. Chem. Int. Ed.* **2019**, *58*, 16644–16650; *Angew. Chem.* **2019**, *131*, 16797–16803.
[82] Y. Zhang, J. Di, P. Ding, J. Zhao, K. Gu, X. Chen, C. Yan, S. Yin, J. Xia, H. Li, *J. Colloid Interface Sci.* **2019**, *553*, 530–539.
[83] S. Wu, Z. Chen, K. Liu, W. Yue, L. Wang, J. Zhang, *ChemSusChem* **2020**, *13*, 3455–3461.
[84] P. Zhou, Y. Chao, F. Lv, J. Lai, K. Wang, S. Guo, *Sci. Bull.* **2020**, *65*, 720–725.
[85] J. Yuan, X. Yi, Y. Tang, M. Liu, C. Liu, *Adv. Funct. Mater.* **2020**, *30*, 1906983.
[86] X. Yao, W. Zhang, J. Huang, Z. Du, X. Hong, X. Chen, X. Hu, X. Wang, *Appl. Catal. A* **2020**, *601*, 117647.
[87] P. Qiu, Z. Liang, X. Liu, X. Qian, H. Cui, J. Tian, *J. Colloid Interface Sci.* **2020**, *571*, 318–325.
[88] Y. Shiraishi, K. Chishiro, S. Tanaka, T. Hirai, *Langmuir* **2020**, *36*, 734–741.
[89] S. Cao, B. Fan, Y. Feng, H. Chen, F. Jiang, X. Wang, *Chem. Eng. J.* **2018**, *353*, 147–156.
[90] Y. Shiraishi, S. Shiota, Y. Kofuji, M. Hashimoto, K. Chishiro, H. Hirakawa, S. Tanaka, S. Ichikawa, T. Hirai, *ACS Appl. Mater. Interfaces* **2018**, *1*, 4169–4177.
[91] A. Shi, H. Li, S. Yin, Z. Hou, J. Rong, J. Zhang, Y. Wang, *Appl. Catal. B* **2018**, *235*, 197–206.
[92] S. Cao, N. Zhou, F. Gao, H. Chen, F. Jiang, *Appl. Catal. B* **2017**, *218*, 600–610.
[93] X. Feng, H. Chen, F. Jiang, X. Wang, *Chem. Eng. J.* **2018**, *347*, 849–859.
[94] Q. Zhang, S. Hu, Z. Fan, D. Liu, Y. Zhao, H. Ma, F. Li, *Dalton Trans.* **2016**, *45*, 3497–3505.
[95] X. Feng, H. Chen, F. Jiang, X. Wang, *J. Colloid Interface Sci.* **2018**, *509*, 298–306.
[96] X. Gao, Y. Wen, D. Qu, L. An, S. Luan, W. Jiang, X. Zong, X. Liu, Z. Sun, *ACS Sustainable Chem. Eng.* **2018**, *6*, 5342–5348.
[97] Y. Zhao, R. Shi, X. Bian, C. Zhou, Y. Zhao, S. Zhang, F. Wu, G. I. N. Waterhouse, L. Wu, C. Tung, T. Zhang, *Adv. Sci.* **2019**, *6*, 1802109.
[98] G. Y. Duan, Y. Ren, Y. Tang, Y. Z. Sun, Y. M. Chen, P. Y. Wan, X. J. Yang, *ChemSusChem* **2020**, *13*, 88–96.
[99] F. Guba, Ü. Tastan, K. Gugeler, M. Buntrock, T. Rommel, D. Ziegenbalg, *Chem. Ing. Tech.* **2018**, *91*, cite.201800035.
[100] M. D. Wilkinson, M. Dumontier, Ij. J. Aalbersberg, G. Appleton, M. Axton, A. Baak, N. Blomberg, J.-W. Boiten, L. B. da Silva Santos, P. E. Bourne, J. Bouwman, A. J. Brookes, T. Clark, M. Crosas, I. Dillo, O. Dumon, S. Edmunds, C. T. Evelo, R. Finkers, A. Gonzalez-Beltran, A. J. G. Gray, P. Groth, C. Goble, J. S. Grethe, J. Heringa, P. A. 't Hoen, R. Hooft, T. Kuhn, R. Kok, J. Kok, S. J. Lusher, M. E. Martone, A. Mons, A. L. Packer, B. Persson, P. Rocca-Serra, M. Roos, R. van Schaik, S.-A. Sansone, E. Schultes, T. Sengstag, T. Slater, G. Strawn, M. A. Swertz, M. Thompson, J. van der Lei, E. van Mulligen, J. Velterop, A. Waagmeester, P. Wittenburg, K. Wolstencroft, J. Zhao, B. Mons, *Sci. Data* **2016**, *3*, 160018.
[101] U. I. Kramm, R. Marschall, M. Rose, *ChemCatChem* **2019**, *11*, 2563–2574.
[102] H. Kisch, *Angew. Chem. Int. Ed.* **2013**, *52*, 812–847; *Angew. Chem.* **2013**, *125*, 842–879.
[103] X. Ye, X. Yan, X. Chu, S. Zuo, W. Liu, X. Li, C. Yao, *Front. Mater.* **2020**, *14*, 469–480.
[104] M. Sender, D. Ziegenbalg, *Chem. Ing. Tech.* **2017**, *89*, 1159–1173.
[105] B. Wriedt, D. Kowalczyk, D. Ziegenbalg, *ChemPhotoChem* **2018**, *2*, 913–921.
[106] B. Wriedt, D. Ziegenbalg, *J. Flow Chem.* **2020**, *10*, 295–306; M. Sender, B. Wriedt, D. Ziegenbalg, *React. Chem. Eng.* **2021**, 10.1039/D0RE00456A; M. Sender, D. Ziegenbalg, *React. Chem. Eng.* **2021**, 10.1039/D0RE00457J.
[107] ASTM International, **2020**, DOI: 10.1520/G0173-03R20.
[108] C. M. Thacker, H. O. Folkins, E. L. Miller, *Ind. Eng. Chem.* **1941**, *33*, 584–590.
[109] C. Xiao, H. Hu, X. Zhang, D. R. MacFarlane, *ACS Sustainable Chem. Eng.* **2017**, *5*, 10858–10863.
[110] C. Zhang, G. Chen, C. Lv, Y. Yao, Y. Xu, X. Jin, Q. Meng, *ACS Sustainable Chem. Eng.* **2018**, *6*, 11190–11195.
[111] A. Shi, H. Li, S. Yin, Z. Hou, J. Rong, J. Zhang, Y. Wang, *Appl. Catal. B* **2018**, *235*, 197–206.
[112] V. Devthade, A. Gupta, S. S. Umare, *ACS Appl. Nano Mater.* **2018**, *1*, 5581–5588.
[113] Q. Liu, L. Ai, J. Jiang, *J. Mater. Chem. A* **2018**, *6*, 4102–4110.
[114] P. Xing, P. Chen, Z. Chen, X. Hu, H. Lin, Y. Wu, L. Zhao, Y. He, *ACS Sustainable Chem. Eng.* **2018**, *6*, 14866–14879.
[115] X. Li, C. He, S. Zuo, X. Yan, D. Dai, Y. Zhang, C. Yao, *Sol. Energy* **2019**, *191*, 251–262.
[116] X. Gao, Y. Shang, L. Liu, F. Fu, *J. Colloid Interface Sci.* **2019**, *533*, 649–657.
[117] J. Liu, R. Li, X. Zu, X. Zhang, Y. Wang, Y. Wang, C. Fan, *Chem. Eng. J.* **2019**, *371*, 796–803.
[118] X. Xue, R. Chen, C. Yan, Y. Hu, W. Zhang, S. Yang, L. Ma, G. Zhu, Z. Jin, *Nanoscale* **2019**, *11*, 10439–10445.
[119] G. Wu, L. Yu, Y. Liu, J. Zhao, Z. Han, G. Geng, *Appl. Surf. Sci.* **2019**, *481*, 649–660.
[120] X. H. Li, W. L. Chen, P. He, T. Wang, D. Liu, Y. W. Li, Y. G. Li, E. B. Wang, *Inorg. Chem. Front.* **2019**, *6*, 3315–3326.
[121] X. Gao, Y. Shang, L. Liu, F. Fu, *J. Catal.* **2019**, *371*, 71–80.
[122] X.-H. H. Li, W.-L. L. Chen, H.-Q. Q. Tan, F.-R. R. Li, J.-P. P. Li, Y.-G. G. Li, E.-B. B. Wang, *ACS Appl. Mater. Interfaces* **2019**, *11*, 37927–37938.
[123] S. X. Wang, H. Maimaiti, B. Xu, Y. Guo, P. S. Zhai, H. Z. Zhang, *J. Phys. Chem. C* **2019**, *123*, 31119–31129.
[124] H. Xu, Y. Wang, X. Dong, N. Zheng, H. Ma, X. Zhang, *Appl. Catal. B* **2019**, *257*, 117932.
[125] C. Zhang, Y. Xu, C. Lv, X. Zhou, Y. Wang, W. Xing, Q. Meng, Y. Kong, G. Chen, *ACS Appl. Mater. Interfaces* **2019**, *11*, 29917–29923.
[126] Z. Zhao, S. Hong, C. Yan, C. Choi, Y. Jung, Y. Liu, S. Liu, X. Li, J. Qiu, Z. Sun, *Chem. Commun.* **2019**, *55*, 7171–7174.
[127] J. Li, P. Liu, Y. Tang, H. Huang, H. Cui, D. Mei, C. Zhong, *ACS Catal.* **2020**, *10*, 2431–2442.
[128] T. Wang, J. Liu, P. Wu, C. Feng, D. Wang, H. Hu, G. Xue, *J. Mater. Chem. A* **2020**, *8*, 16590–16598.
[129] S. Mansingh, S. Sultana, R. Acharya, M. K. Ghosh, K. M. Parida, *Inorg. Chem.* **2020**, *59*, 3856–3873.
[130] S. Bian, M. Wen, J. Wang, N. Yang, P. K. Chu, X. F. Yu, *J. Phys. Chem. Lett.* **2020**, *11*, 1052–1058.
[131] E. Vesali-Kermani, A. Habibi-Yangjeh, H. Diarmand-Khalilabad, S. Ghosh, *J. Colloid Interface Sci.* **2020**, *563*, 81–91.
[132] E. Vesali-Kermani, A. Habibi-Yangjeh, S. Ghosh, *J. Ind. Eng. Chem.* **2020**, *84*, 185–195.
[133] E. Vesali-Kermani, A. Habibi-Yangjeh, S. Ghosh, *Ceram. Int.* **2020**, *46*, 24472–24482.
[134] Y. Kong, C. Lv, C. Zhang, G. Chen, *Appl. Surf. Sci.* **2020**, *515*, 146009.
[135] S. Wu, Z. Chen, K. Liu, W. Yue, L. Wang, J. Zhang, *ChemSusChem* **2020**, *13*, 3455–3461.
[136] S. Zhang, Y. Zhao, R. Shi, C. Zhou, G. I. N. Waterhouse, L. Z. Wu, C. H. Tung, T. Zhang, *Adv. Energy Mater.* **2020**, *10*, 1901973.
[137] J. Wang, C. Hua, X. Dong, Y. Wang, N. Zheng, *Sustain. Energy Fuels* **2020**, *4*, 1855–1862.
[138] X. H. Li, P. He, T. Wang, X. W. Zhang, W. L. Chen, Y. G. Li, *ChemSusChem* **2020**, *13*, 2769–2778.

[139] P. Xing, W. Zhang, L. Chen, X. Dai, J. Zhang, L. Zhao, Y. He, *Sustain. Energy Fuels* **2020**, *4*, 1112–1117.
[140] C. Hao, Y. Liao, Y. Wu, Y. An, J. Lin, Z. Gu, M. Jiang, S. Hu, X. Wang, *J. Phys. Chem. Solids* **2020**, *136*, 109141.
[141] H. Huang, X.-S. S. Wang, D. Philo, F. Ichihara, H. Song, Y. Li, D. Li, T. Qiu, S. Wang, J. Ye, *Appl. Catal. B* **2020**, *267*, 118686.
[142] G. Zhang, X. Yang, C. He, P. Zhang, H. Mi, *J. Mater. Chem. A* **2020**, *8*, 334–341.
[143] T. Hou, Q. Li, Y. Zhang, W. Zhu, K. Yu, S. Wang, Q. Xu, S. Liang, L. Wang, *Appl. Catal. B* **2020**, *273*, 119072.
[144] K. Takanabe, *ACS Catal.* **2017**, *7*, 8006–8022.
[145] I. Reim, B. Wriedt, Ü. Tastan, D. Ziegenbalg, M. Karnahl, *ChemistrySelect* **2018**, *3*, 2905–2911.
[146] F. Zhao, D. Cambié, V. Hessel, M. G. Debije, T. Noël, *Green Chem.* **2018**, *20*, 2459–2464.
[147] X. Chen, S. Shen, L. Guo, S. S. Mao, *Chem. Rev.* **2010**, *110*, 6503–6570.
[148] H. Kato, K. Asakura, A. Kudo, *J. Am. Chem. Soc.* **2003**, *125*, 3082–3089.
[149] T. Takata, J. Jiang, Y. Sakata, M. Nakabayashi, N. Shibata, V. Nandal, K. Seki, T. Hisatomi, K. Domen, *Nature* **2020**, *581*, 411–414.
[150] Q. Wang, T. Hisatomi, Q. Jia, H. Tokudome, M. Zhong, C. Wang, Z. Pan, T. Takata, M. Nakabayashi, N. Shibata, Y. Li, I. D. Sharp, A. Kudo, T. Yamada, K. Domen, *Nat. Mater.* **2016**, *15*, 611–615.
[151] Y. Ren, C. Yu, X. Tan, H. Huang, Q. Wei, J. Qiu, *Energy Environ. Sci.* **2021**, *14*, 1176–1193.
[152] C. Tang, S.-Z. Qiao, *Chem. Soc. Rev.* **2019**, *48*, 3166–3180.
[153] H. Idriss, *Catal. Sci. Technol.* **2020**, *10*, 304–310.

Manuscript received: April 15, 2021
Revised manuscript received: May 31, 2021
Accepted manuscript online: June 1, 2021
Version of record online: July 8, 2021